10-2022

# The Effect of Specimen Thickness on the Lüders Phenomena in AISI 1524 Steel Alloy

Joost H. van der Heijde
jxv2643@rit.edu

# The Effect of Specimen Thickness on the Lüders Phenomena in AISI 1524 Steel Alloy

By

Joost H. van der Heijde

A Thesis Submitted

in Partial Fulfillment

of the Requirements for the Degree of

Master of Science

in

Mechanical Engineering

Approved by:

Prof. _____
Dr. Wael A. Samad (Thesis Advisor)

Prof. _____
Dr. Rui Liu (Committee Member)

Prof. _____
Dr. Salman Pervaiz (Committee Member)

DEPARTMENT OF MECHANICAL ENGINEERING

KATE GLEASON COLLEGE OF ENGINEERING

ROCHESTER INSTITUTE OF TECHNOLOGY

DUBAI, UNITED ARAB EMIRATES

OCTOBER, 2022

# Acknowledgements

I would like to firstly thank my advisor, Dr. Wael A. Samad, for his guidance, support, and patience during my thesis research. His expertise in experimental mechanics and advice on research in general was invaluable. I would also like to express my gratitude to the committee members, Dr. Rui Liu and Dr. Salman Pervaiz, for their feedback on my work and insightful advice.

I would further like to thank Raviprakash and Abhishek from Pyrodynamics for their technical assistance in providing access to the required DIC software. I am also grateful to Dr. Priyank Upadhyaya and Sudip Baul from BITS Pilani, Dubai Campus for allowing access to their Digital Microscope and lab facilities for this study.

# Abstract

At certain temperatures, strain rates and slender geometries, low carbon steels, as well as some aluminum, magnesium and nickel-based alloys, exhibit plastic flow instability at the onset of their respective yield points, known as the Lüders phenomena. Such phenomenon is recognized by a distinct yield point and subsequent plateau on the stress-strain curve. This thesis aims to investigate the effect of the sample's thickness on the Lüders phenomena in AISI 1524 hot-rolled steel alloy. Sixteen samples were machined from hot-rolled plates and uniaxial testing in conjunction with digital image correlation were performed to gain insight and quantify the Lüders band's characteristics during the extent of the plateau. The thicknesses investigated were 1 mm, 2 mm, 3 mm, and 4 mm, all of which tested under identical conditions, most notably strain rate, in order to isolate and understand the effect of material's thickness on the Lüders phenomena. Results revealed that an increase in specimen thickness resulted in an increase in Lüders band width as well as an increase in Lüders band velocity in 1524 steel alloy. Results also showed that a dual band formation took place in all samples regardless of thickness. Moreover, the angle at which the Lüders band appeared on the front surface of the specimen increased with increasing structure thickness. The obtained results and observations suggested a 3D nature of the band's formation in AISI 1524; whereby nucleation takes place at the core of the material before propagating in the thickness direction towards the structure's surface. Moreover, it was concluded that the Lüders band initiated ahead of the upper yield stress point.

## Research Aim

Lüders band formation can pose problems in metal forming. For example, when you plastically deform sheet steel to make a car fender, the formation of Lüders bands will cause ripples on the surface rendering the part as scrap. This work aims to investigate the specimen thickness dependence of the Lüders effect in mild steel-based alloys, specifically on Lüders band formation, size, and rate of propagation during the extent of the plateau, by utilizing uniaxial testing in conjunction with digital image correlation. Gaining further insight into the effects of the Lüders phenomena can lead to improvement of current design models and codes, leading to less residual stresses in materials and reducing the amount of conservatism required in a design.

# Table of Contents

# List of Figures

# Chapter 1. Introduction

At certain temperatures and strain rates, low carbon steels, as well as some aluminum and magnesium-based alloys, exhibit plastic flow instability at the onset of their respective yield points, known as the Lüders phenomena. Such an effect is recognized by a distinct yield point and subsequent plateau on the stress-strain curve, and takes the form of a band when full-field tensile strains are observed experimentally. Lüders band, and in some cases bands, typically initiate from the regions of the specimen held in the grips and propagate from one end of the specimen to the other [1]. Recent advancements in the area of full-field displacement-based methods have led to several investigations into the Lüders phenomenon. Such methods and experimental techniques include surface coating [2], strain gages [3], infrared thermography [4] and of course, more recently using digital image correlation (DIC), the more prevalent method given its relative ease and more importantly its full-field displacement and strain nature. This work aims to investigate the specimen thickness dependence of the Lüders effect in mild steel-based alloys, specifically on Lüders band formation, size, and rate of propagation during the extent of the plateau, by utilizing uniaxial testing in conjunction with digital image correlation. Gaining further insight into the effects of the Lüders phenomena can lead to improvement of current design models and codes, leading to less residual stresses in materials and reducing the amount of conservatism required in a design.

The Lüders effect is caused by a combination of collective dislocation multiplication and motion, and the dislocation pinning/unpinning effect arising from Cottrell atmosphere constraints. According to work by Cottrell on iron, yielding starts in highly stressed regions and is propagated

in the form of Lüders bands from these regions along the specimen. At the lower yield point, elastic disturbance due to nearby plastic flow helps the release of dislocations at the edges of the Lüders bands [5].

Work by Rešković et al. [6] investigated how the tensile test rate affects the formation, propagation, and temperature change of Lüders band on low carbon and niobium micro alloyed steel using thermal imaging. Previous research had only been able to explain the effect of niobium precipitates as a combination of deformation mechanisms, which lead the authors to investigate the beginning of the plastic flow in niobium micro alloyed steel. Tensile testing was performed with rates ranging from 5 to 30 mm/s, and elongation and temperature data was recorded using an infrared camera.

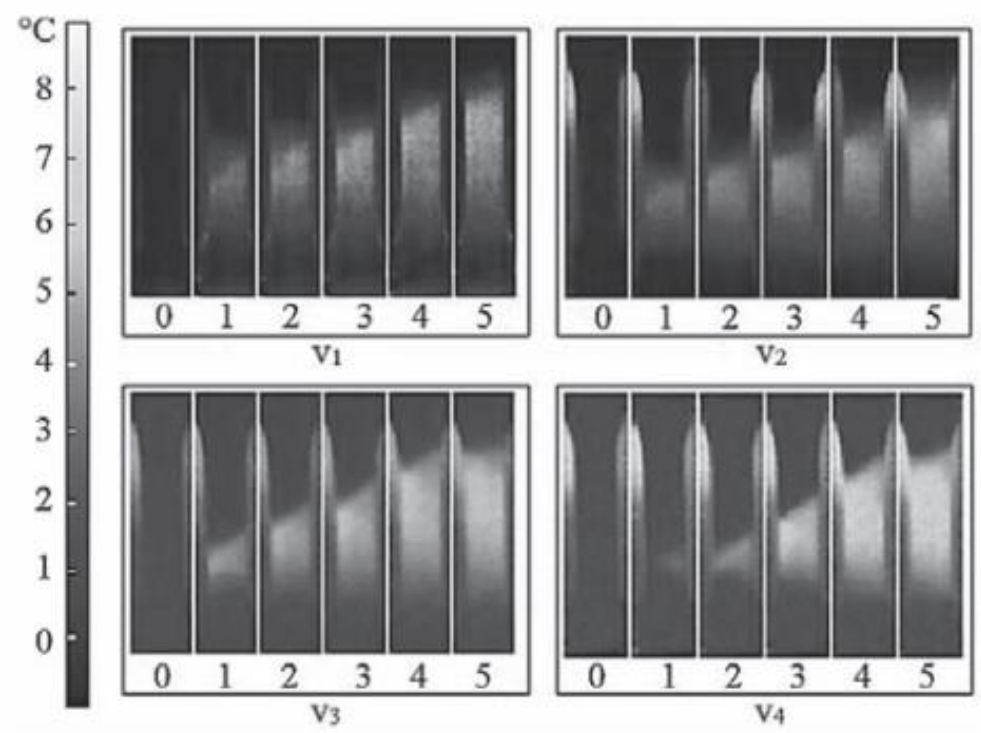


*Figure 1 - Propagation of Lüders bands [6]*

Figure 1 shows the temperature increase in the deformation area which propagates at a 45-degree angle. The moving thermal front shows the formation of Lüders band. The authors concluded that the propagation velocity of Lüders band is highly dependent on the applied strain rate.

Similarly, work by Cai et al. [7] used 3D-DIC to examine the effect that varying the specimen thickness in a 5456-aluminum alloy had on the Lüders band velocity, strain, and the correlation between the two. Previous research had shown the influence of thickness of copper whiskers on plastic behavior at a micrometer scale. This work continues on recent research on thickness dependence in various materials on a millimeter scale. Uniaxial tensile testing was performed on

specimens with thicknesses of 1, 2, and 3 mm while using 3D-DIC technique to capture full-field displacement and strain.

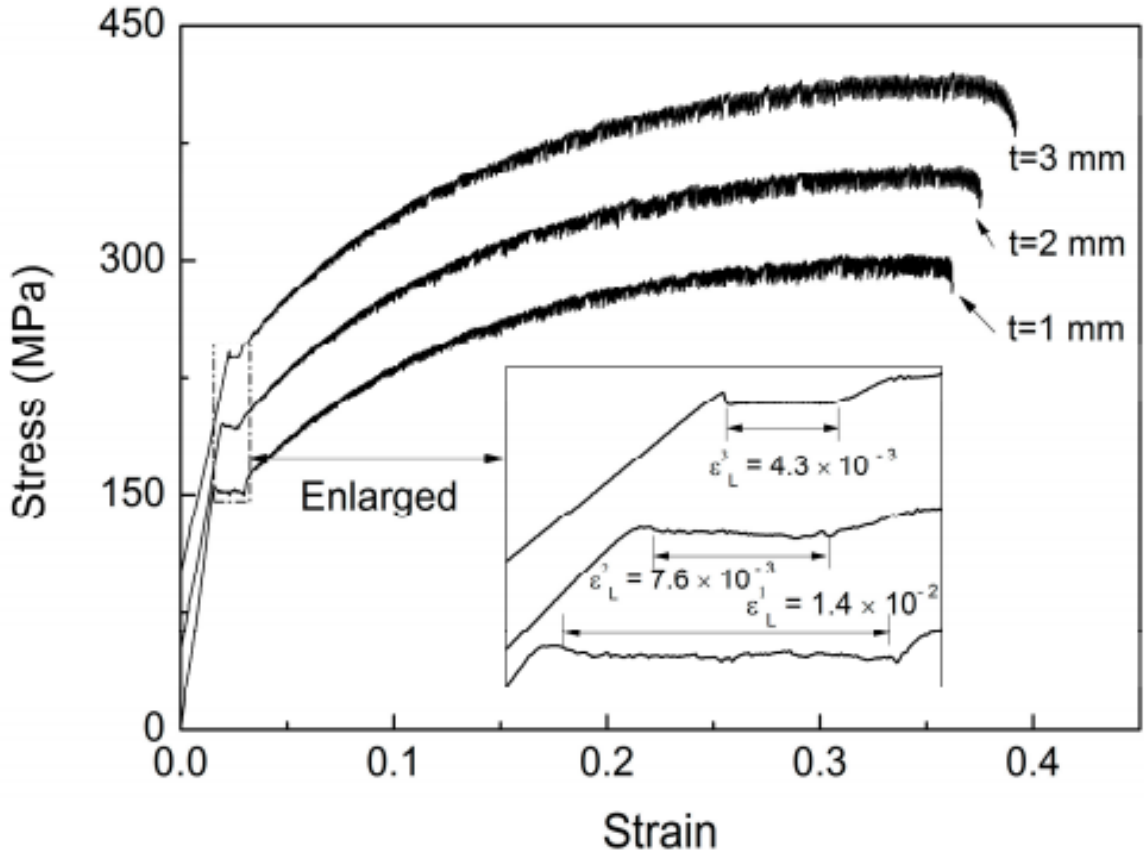


*Figure 2 - Stress-strain curves for specimens with varying thicknesses [7]*

Figure 2 displays the stress-strain curves for specimens with varying thicknesses, separated in 35 MPa stress intervals for clarity. Lüders plateau is clearly shown in the magnified view, whereby increased specimen thickness leads to a decreased length of the plateau. The authors further concluded that a decrease in specimen thickness leads to a reduction in Lüders band velocity. The

dependence of the Lüders band velocity and the Lüders strain on the specimen thickness at a fixed strain rate is further shown in Figure 3.

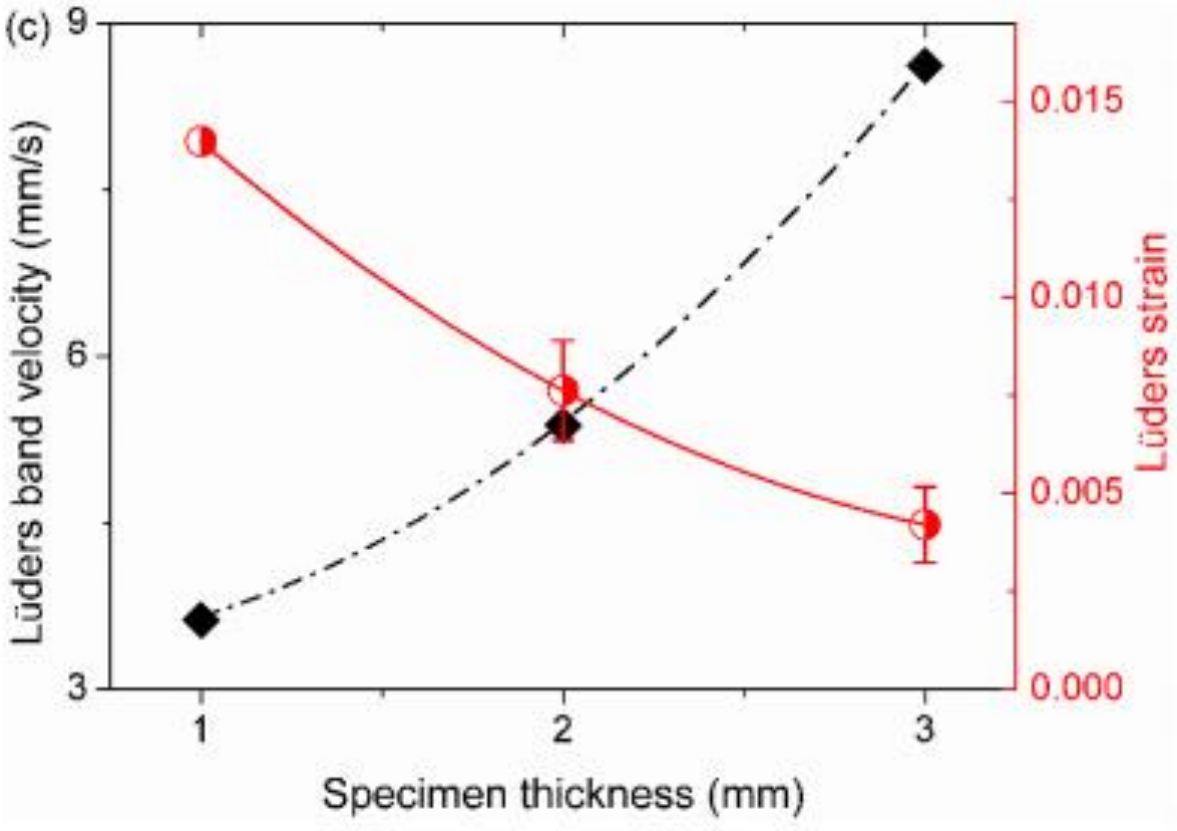


*Figure 3 - Dependence of the Lüders band velocity and the Lüders strain on the specimen thickness, at a fixed strain rate [7]*

Sun et al. [8] utilized uniaxial tension testing on annealed mild steel to investigate the effect varying the strain rate on Lüders strain and the propagation velocity of Lüders band. Past research by Sylwestrowicz et al. [9] had found empirical equations for Lüders strain, but no physical-based equations were derived thus far. Physical equations (exponent functions) have been proposed and verified experimentally in this work to express behavior of Lüders strain and band velocity

behavior. Uniaxial tests at varying crosshead speeds were performed on low carbon sheet and round wire specimens.

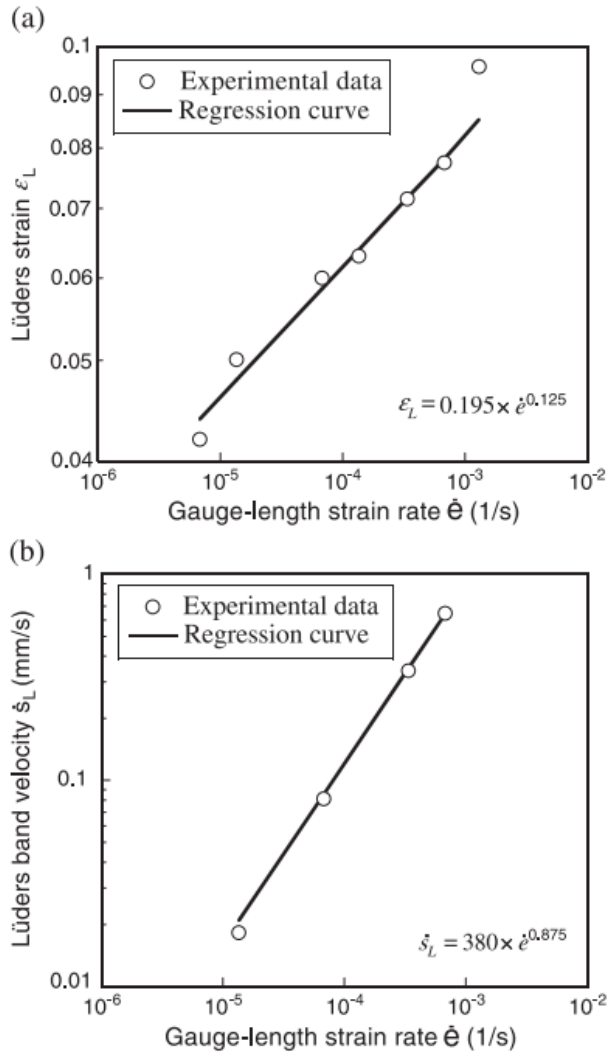


*Figure 4 - Experimental data to demonstrate validity of equations [8]*

Figure 4 displays the experimental data to demonstrate the validity of the equations for Lüders strain and Lüders-band velocity for the sheet specimen, although similar results are provided round

wire specimen. The experimental and regression data correlated well and thereby validates the equations.

Similar work by Zhang et al. [10] investigated the propagation of Lüders band in 145-steel under multiaxial stress state. Thin-walled tubular specimens were subjected to different loading scenarios while strain gauges were mounted on the specimen's surface. Monotonic tension, monotonic torsion, proportional tension-torsion, and monotonic torsion with a constant axial load experiments were performed. Figure 5 displays the tensile stress-extensometer strain curve and variation of location axial strains for the specimen under monotonic tension.

The authors found deformation to occur in two stages, namely first rapid deformation, followed by a slow deformation process. It was found that under tension, torsion, and constant axial load tension-torsion, multiple Lüders fronts can be formed during the propagation of Lüders band, and that the maximum shear stress was nearly parallel with the Lüders front. When combined axial-torsion was applied, the propagation and location of Lüders fronts were different. For both loading cases, however, the equivalent plastic strain and stress relationship remained similar.

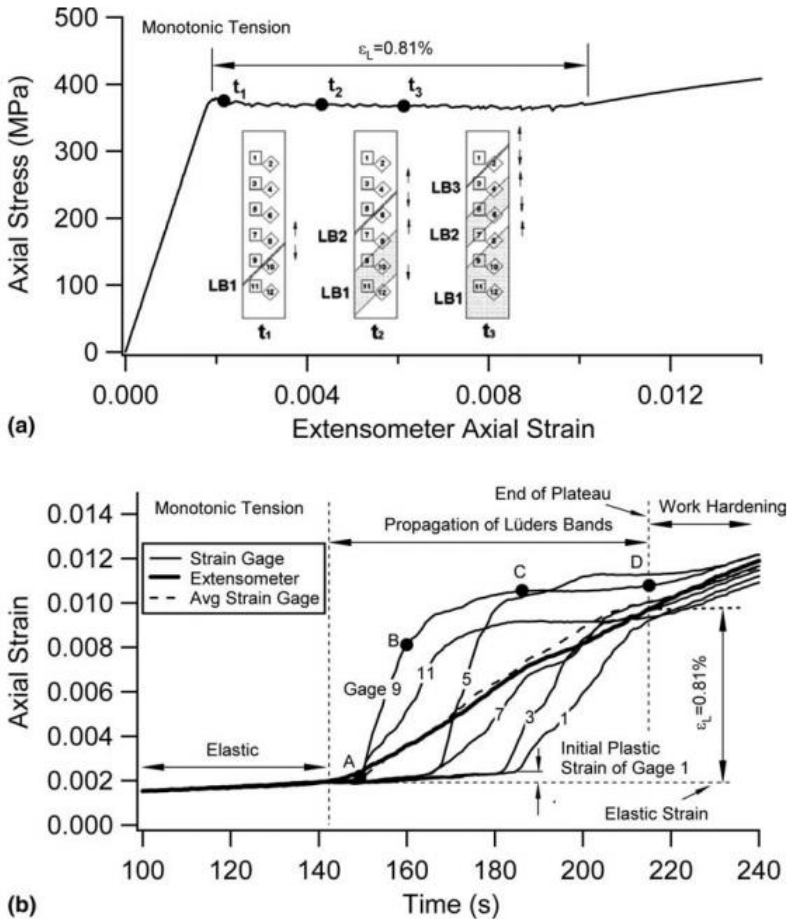


*Figure 5 - Monotonic tension behavior: (a) tensile stress–extensometer strain curve; (b) variation [9]*

Continuing on work by Rešković et al. [9] , Brlić et al. [11] conducted a review on research of Lüders band at the beginning of the plastic flow of materials, specifically what parameters have an effect on the occurrence and propagation of Lüders bands. Common methods include uniaxial tensile tests, thermal image cameras and digital image correlation. Figure 6 shows Lüders band in a specimen using thermography and digital image correlation.

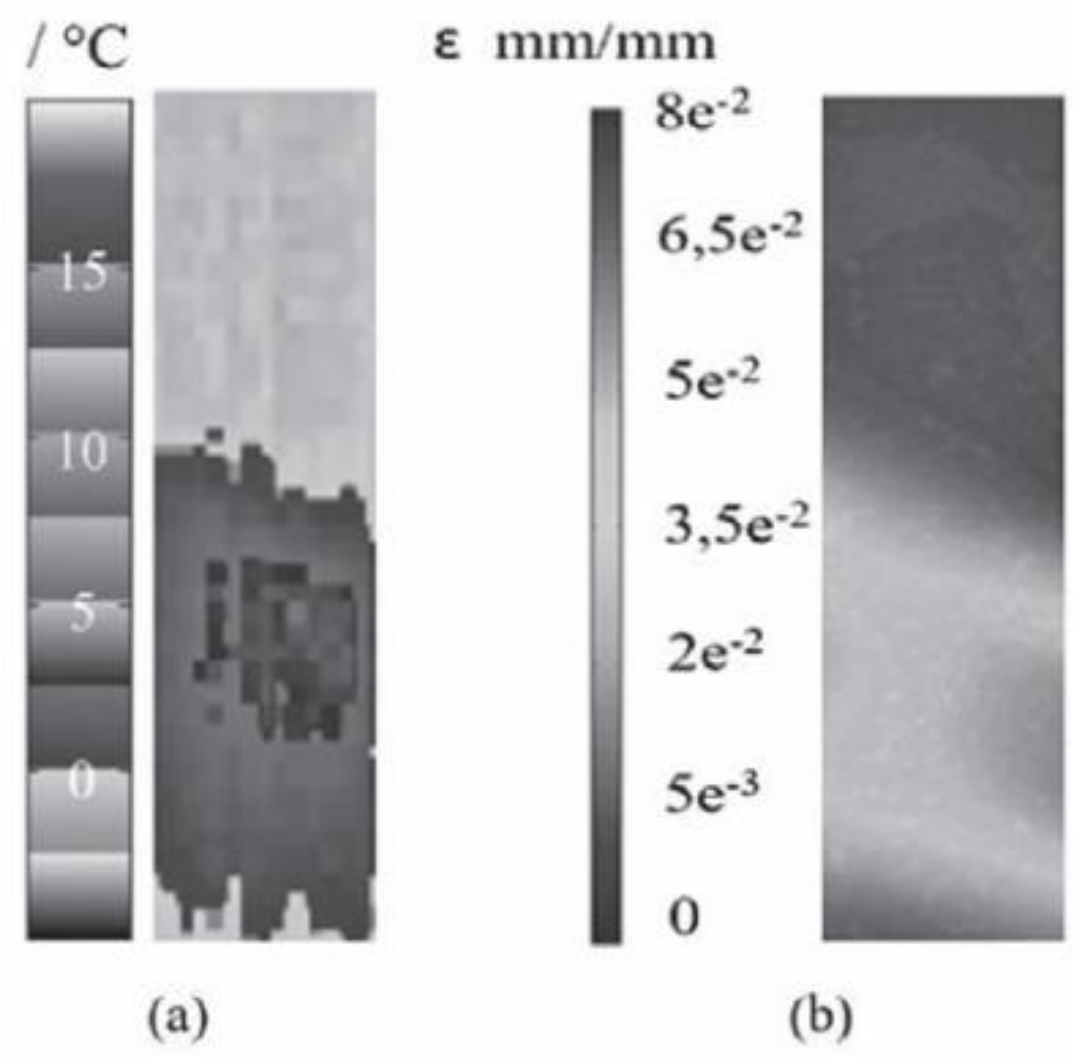


*Figure 6 - Lüders band detection using two methods: a) thermography & b) digital image correlation (DIC) [10]*

The propagation mechanism has been studied quite thoroughly, but no general explanation exists for band formation. A research gap exists in the influence of the chemical composition of materials on the occurrence of Lüders bands. It has been found that the parameters affecting strain vary between materials, therefore being attributed to the chemical composition, whereby the effect of microstructure and grain size is not fully understood. Interestingly from a strength of materials

point of view, a research gap exists on the effect of specimen thickness and strain rate on materials with a different chemical composition.

A topic that frequently appears in literature on Lüders effect is the Portevin-Le Chatelier (PLC) effect. The PLC effect can be denoted by a serrated stress-strain curve during plastic deformation. The PLC effect is observed more frequently in AL based alloys. Work by Ren et al. [12] used FE and DIC methods to investigate how PLC and Lüders bands affect fracture and plasticity in notched C-Mn (A42) steel specimens. 3D FE simulations were used to reproduce results of the effect of a notch on PLC localization bands at both high temperatures (as illustrated in Figure 7) and room temperature. The authors found a flat to slant crack transition due to the PLC effect at high temperatures (175 ◦C), and a flat crack at room temperature since only Lüders band is active at such temperatures. Figure 7 illustrates the experimental setup used.

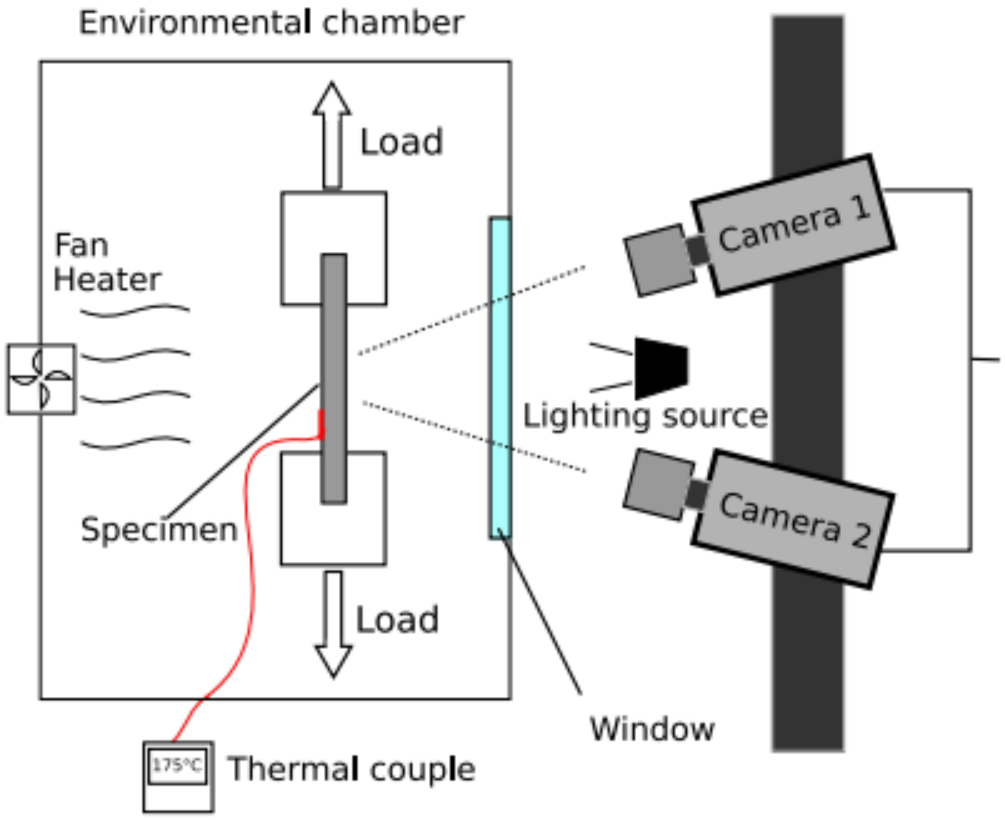


*Figure 7 - DIC setup for high temperature test [11]*

Similarly, work by Reyne et al. [13] investigated the macroscopic effects of PLC and Lüders bands on Al-Mg alloys at room temperature under tensile deformation by investigating the kinetics of individual localization bands using DIC techniques. Although this work focused more heavily on the materials science aspects of these bands, an interesting conclusion is that the distribution of serrations decreased with an increasing strain rate, whereas the individual serrations tend to increase with increasing strain. Furthermore, Lüders behavior was observed only at low strain rate as seen in Figure 8.

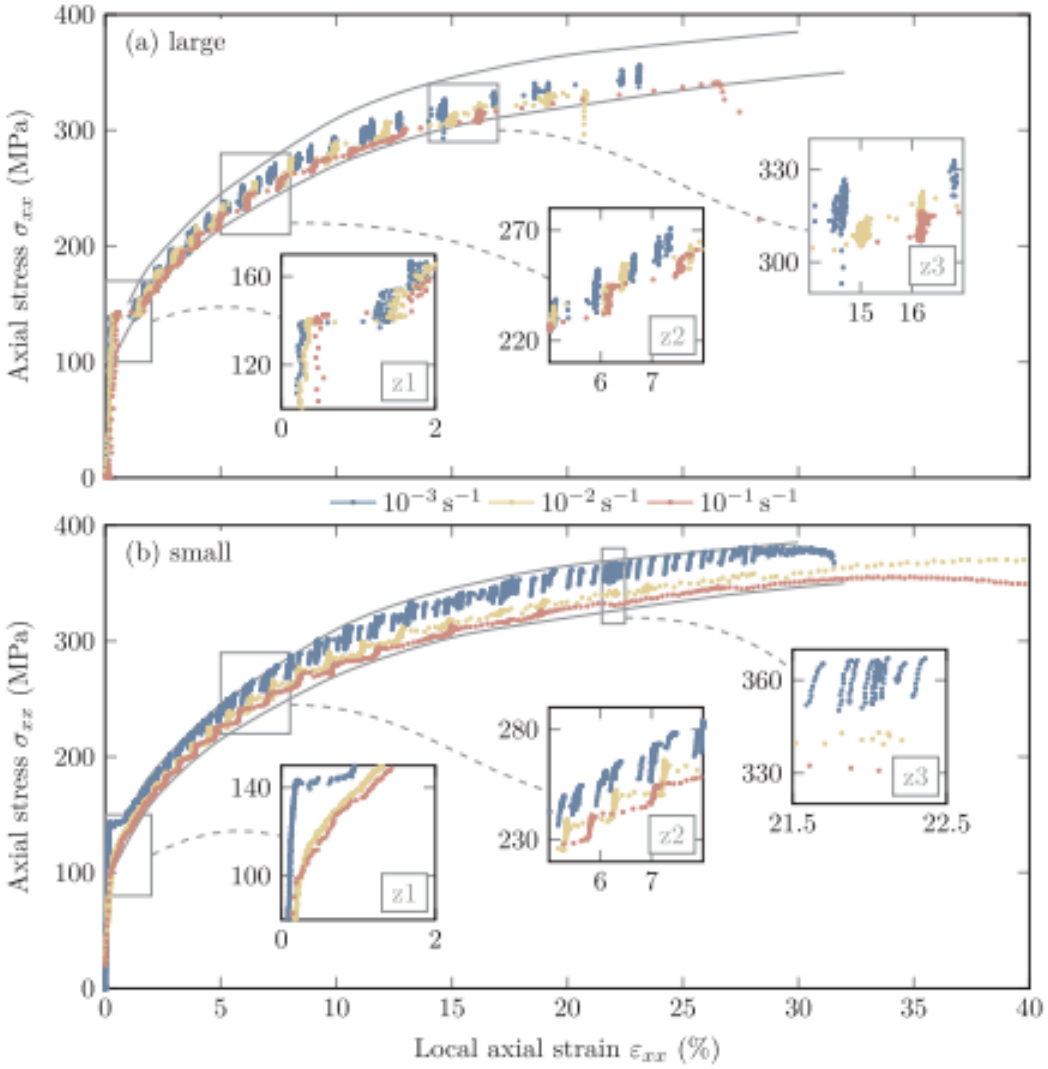


*Figure 8 - Cauchy stress vs. linearized Green–Lagrange strain curves on large (a) and small (b) samples [13]*

More investigations into Al-Mg alloys (a common metal in literature on Lüders and PLC effects) was done by Coër et al. [14] under simple shear tests, again with DIC methods to observe the specimen's surface. In contrast to the work done by Ren et al., where only the Lüders phenomenon was observed at room temperature under tensile testing, both Lüders and PLC effects were observed at room temperature while conducting simple shear tests.

Research performed by Mazière et al. [15] investigated the Lüders effect in low carbon ferritic steel in simple shear loading using experimental and numerical analysis. Based on DIC measurements of tensile and shear tests an elastoviscoplastic constitutive law was formulated, which was then introduced in finite element simulations of shear loading. The authors found some mesh sensitivity while simulating Lüders band in both free and regular meshes, whereby the Lüders band front was reduced to a few lines in both meshes. An additional degree of freedom, called the internal length, was then introduced in a micromeritic model and verified experimentally to obtain a fully mesh insensitive finite element model. Lastly, the authors proposed more realistic boundary condition simulation that accounts for grip tightening, which reduced the Lüders peak in the simulation and brought it closer to experimental values.

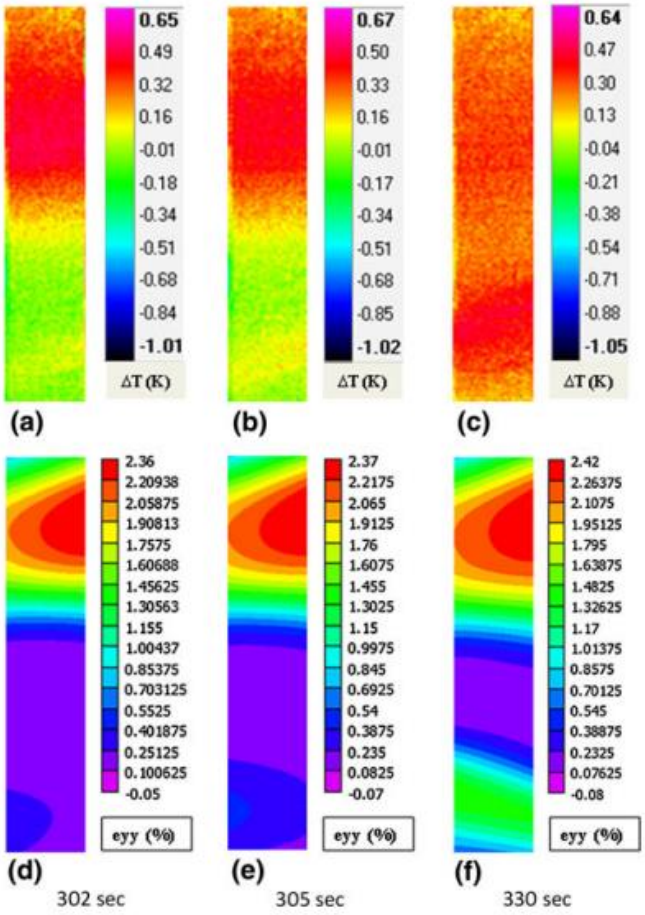


*Figure 9 - Lüders band and the formation of a second band, obtained from both IRT and DIC methods [4]*

Further investigation into Lüders effect using advanced imaging techniques was performed by Nagarajan et al. [4]. The authors combined digital image correlation with infrared thermography to analyze Lüders deformation, an example of which can be seen in Figure 9. Both techniques were used to verify several concepts and proposed models that explain the dynamics of Lüders deformation, such as band formation, strain localization, and nonhomogeneous stress-strain distribution on the band front. This work proved that combining DIC and IRT techniques enables macroscopic strain and thermal investigations to provide a better understanding of the micro mechanisms related to Lüders deformation.

A similar combination of imaging techniques was utilized by Avril et al. [16], whereby DIC measurements were paired with imaging from high-speed CCD cameras taken from tensile loading experiments on steel bars. Non-standard specimens were used to obtain non-uniform strain field measurements within the specimen, which provides sufficient information for characterization of elastoviscoplastic behavior while combing full-field deformation measurements and virtual fields method. Several existing models were evaluated by comparing results from this approach to those obtained with standard dog-bone specimens. Acceptable results were found from Yoshida's model [17], which accounts for Lüders behavior. In this research the authors found that full-field DIC techniques, paired with the correct computational technology (VFM) enables analysis of transient strain localization in high strain rate tensile testing scenarios.

Johnson [18] analyzed Lüders bands in low carbon alloy, reactor pressure vessel (RPV) steel. Previous work proved that residual stresses in the material can be reduced by incorporating Lüders band into the calculations. This research aimed to generalize these findings by looking into failure assessment diagrams. A better understanding of Lüders band was developed by means of a theoretical model which describes the relationship between Lüders strain, grain size, and density of dislocations. Current codes used to design RPVs and predict fracture assume continuous material yields as the size of Lüders strain is less than 2%. Incorporating Lüders band into the model can reduce residual stresses in the material and reduce the level of conservatism needed. This difference may lead to a different approach when designing RPVs with specific properties in relation to Lüders band, whereby other types of steel with a different microstructure could be selected. This work highlights the importance of gaining further insights into factors that affect Lüders bands.

Literature has shown that low carbon steels, as well as some Al and Mg based alloys, exhibit the heterogenous Lüders phenomenon at specific temperatures and strain rates. Research has proven that the Lüders effect is affected by tensile strain rate, impurity concentration in the alloy, test temperature, grain size, and the material's thickness. Recent advancements in full field displacement techniques enable better analysis and quantification of such effect. Gaining further insight into the effects of the Lüders phenomena can lead to improvement of current design models and codes, leading to less residual stresses in materials and reducing the amount of conservatism required in a design. This thesis aims to investigate the specimen thickness dependence of the Lüders effect in AISI 524 hot-rolled steel alloy, specifically on Lüders band formation, spatial features, size, and rate of propagation during the extent of the plateau.

# Chapter 2. Materials and Methods

In the work presented here, the material's thickness effect on the Lüders band is investigated for commercial AISI 1524 hot-rolled mild steel. The material was sourced from the local market in Sharjah, United Arab Emirates, and is widely used in industry throughout the Gulf region. The chemical composition of the steel plates from which the specimens were machined were determined through an optical emission spectroscopy analysis (OES) in accordance to ASTM E415 [19]. The OES chemical composition of the mild steel at hand is listed in Table 1, revealing 0.24C/0.83M/0.031P/0.016S (in wt%) as the main constituents, confirming its AISI 1524 designation.

**Table 1.** Chemical composition (wt. %) of the AISI 1524 alloy.

| **Element** | **C** | **Mn** | **P** | **S** | **Si** | **Cr** | **Ni** | **Mo** | **Cu** | **N** | **V** | **Fe** |
|---|---|---|---|---|---|---|---|---|---|---|---|---|
| Content (wt. %) | 0.24 | 0.83 | 0.031 | 0.016 | 0.08 | 0.03 | 0.03 | 0.007 | 0.008 | 0.008 | 0.001 | Balance |

Further, the grain microstructure of the material was obtained using a Chennai Metco Metscope I optical microscope and is shown in Figure 10. Chennai Metco Envision 6.0 image analysis software was subsequently used on the micrograph to perform grain size (planimetric) analysis in accordance with ASTM standard E112 [20]. The microstructural imaging was performed at the materials laboratory of BITS Pilani, Dubai campus, as this facility is not available at RIT Dubai's laboratories. Therefore, only one thickness was investigated, although the microstructure of the other samples thicknesses are expected to be fairly identical as per the supplier's information. The

average grain size for the AISI 1524 steel under investigation was found to be 11 μm. It is worth noting that while the grain size was not a design parameter in this study, the Lüders phenomena was previously reported to be affected by steel alloy's grain size as shown in [21].

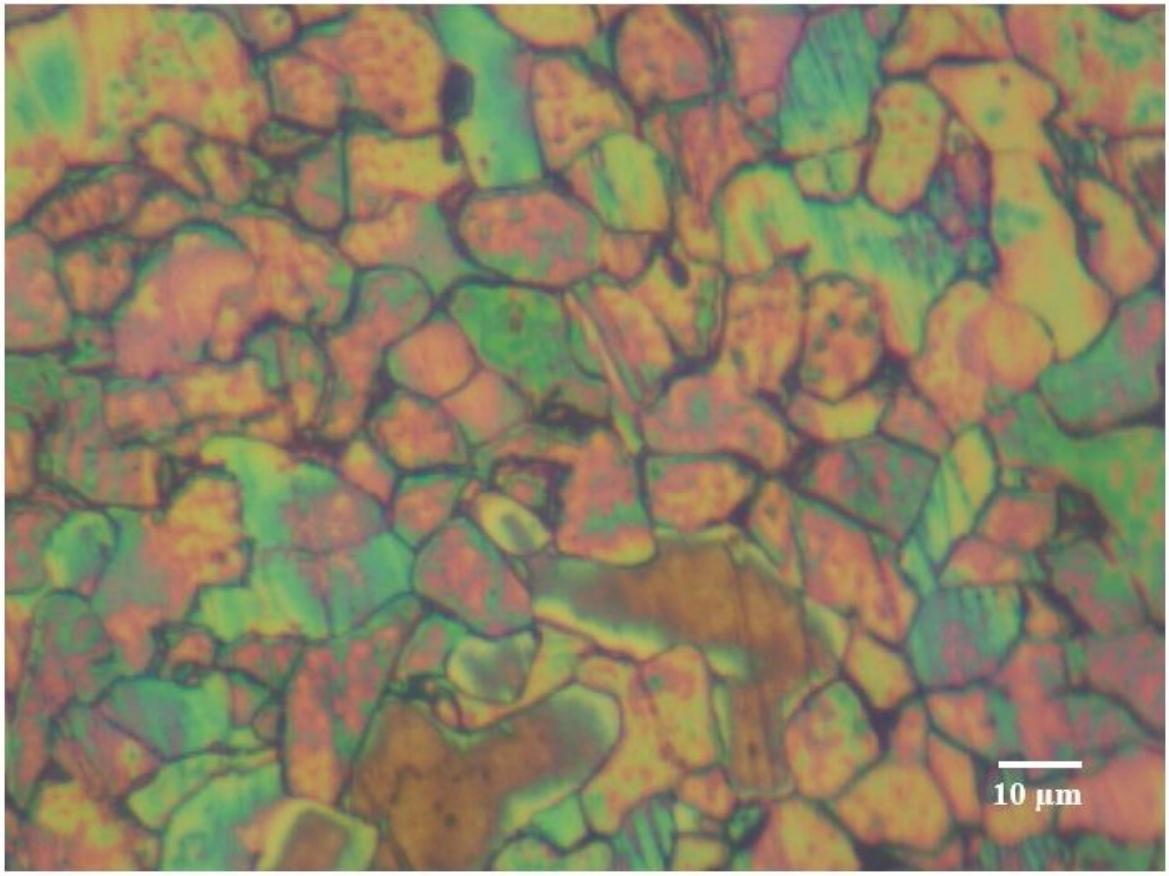


*Figure 10 - Grain microstructure of the AISI 1524 steel alloy under investigation*

In order to investigate the effect of specimen thickness on Lüders effect in low carbon steel alloys, uniaxial testing in conjunction with digital image correlation was employed to capture Lüders band. A total of sixteen dog-bone samples were then machined from four different sheets of the mild steel material with varying thicknesses (1 mm, 2mm, 3 mm and 4 mm), having a gauge length

of 60 mm and a gauge width of 20 mm as shown in Figure 11. Specimen dimensions were kept consistent with the ASTM E8/E8M standard [22], with a slight variation in specimen width of the gauge section from the ASTM sample size. Since a DIC system with fixed camera and focal length were used, it proved difficult to obtain good focus and a sufficient number of data points with a smaller width. In literature, similar sample sizes are used for this reason [7].

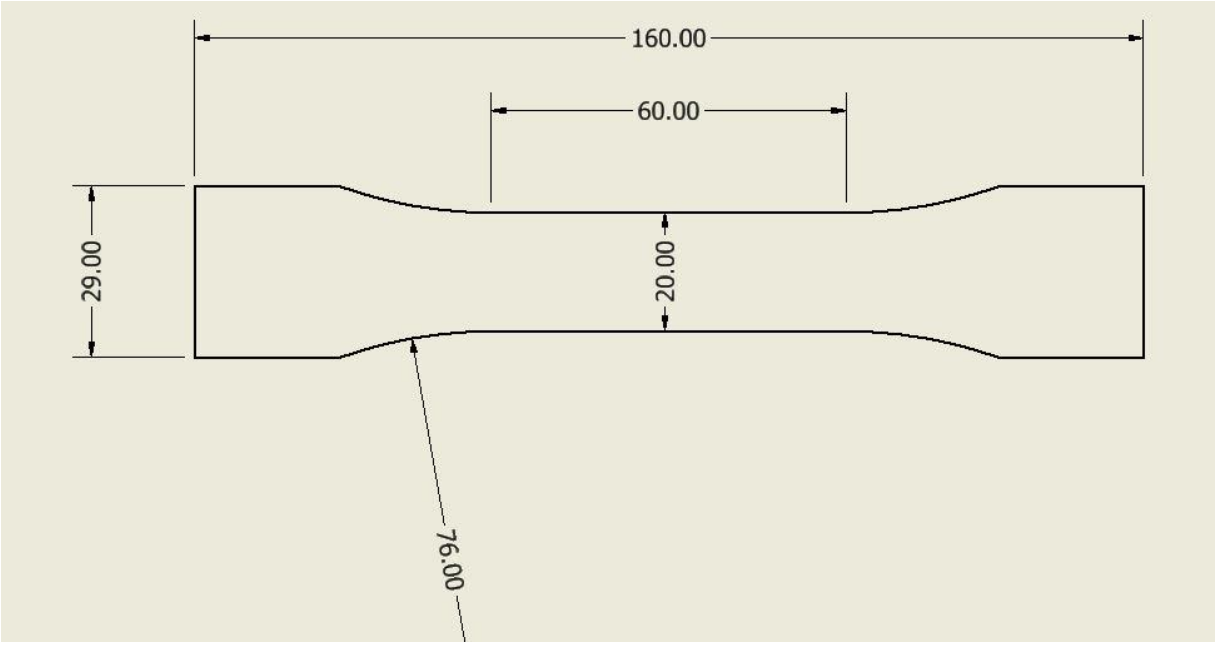


*Figure 11 - Dimensions of dog-bone shaped specimens in mm*

In this research, a digital image correlation (DIC) method will be used to analyze Lüders effect. This technique is used to measure full-field space coordinates, displacement, and strain distributions on a specimen. DIC is an optical measurement technology which measures deformation on the surface of an object. Using subsets (gray value patterns in a selected area) DIC

can track changes while an object is undergoing deformation. Figure 12 show two examples of a subset with the gray value pattern highlighted in green and red.

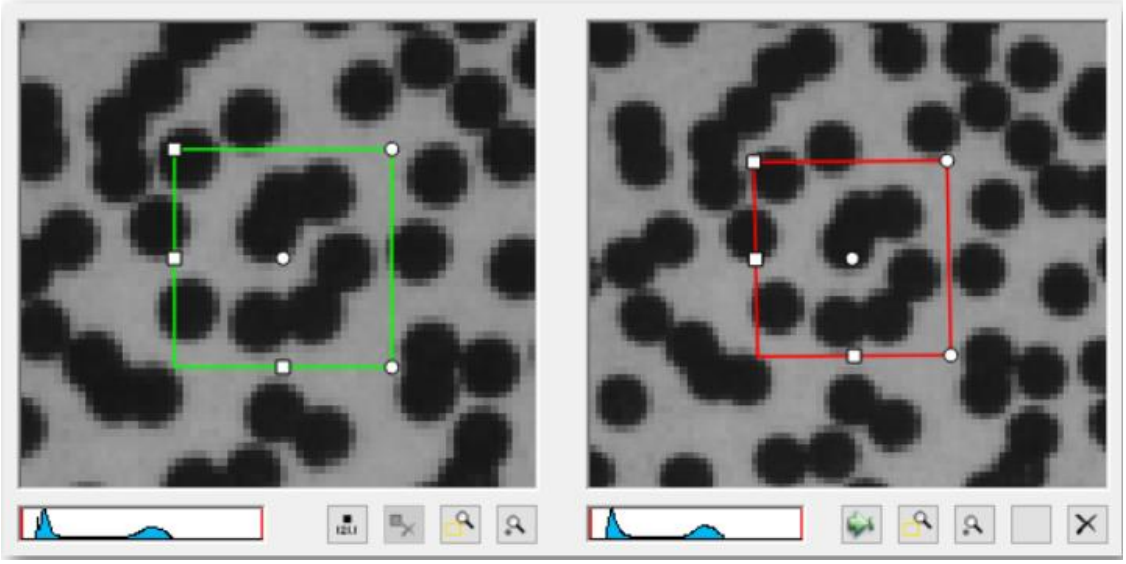

*Figure 12 - Gray value pattern in subsets [23]*

The DIC system consists of 2 cameras with a light source and obtains direct images of a randomized speckle pattern that is applied on a specimen. These images can then later be used in quantitative analysis. In this study, a VIC-3D Educational System by correlated Solutions will be utilized. Although the system can provide three-dimensional information due to the stereo-system setup with two cameras, the deformation in this study is mainly in-plane, and images from a single camera were used to measure deformation. This system requires manual calibration of location, camera orientation, focus, and lighting conditions prior to use. The accompanying VIC-3D software was used for tracking the speckles and to provide data on displacement and strain distributions on the specimens.

*Figure 13 - Unpainted coupons of 1-4 mm*

The dog-bone specimens underwent various procedures in preparation for DIC testing. First, the specimens were first gently cleaned and polished using sandpaper and then degreased, as shown in Figure 13. Special care was taken during this process so as to maintain the samples' thickness. After which, a thin layer of white spray paint was uniformly applied using a matt white spray paint bottle, the result of which is shown in Figure 15. Once the white paint dried out, a random pattern of speckles (i.e. black dots) were applied manually using a fine-tip black marker whilst ensuring to a great extent an even speckle size as well as random locations. The speckle pattern applied here was in line with the recommended practices documented in the Correlated Solutions testing guide [24]. More specifically, the speckle pattern I applied was isotropic (i.e. showing no direction bias), was randomly applied (i.e. showing no pattern or grid like behavior) and had a fairly consistent

speckle size, coverage and contrast throughout. Those are important in order to reduce the measurement noise and improve the overall DIC correlated results. An example of the speckled-painted samples is shown in Figure 16 and Figure 18. Special care was taken to obtain an optimal pattern (i.e. speckles that are neither too large nor too small). The propagation of a subset of the image is tracked, as the object deforms, by shifting the subset until the pattern of the deformed image closely resembles that of the reference image. With a subset that's too small, or a pattern that's too large, significant black or white areas may occur, preventing a good match. With a pattern that's too small, aliasing may occur due to hardware limitations (i.e. camera resolution): a jittery pattern will be observed and large grey areas may appear [25]. Figure 14 shows examples of subsets with speckles that are too small or too large, resulting into large area black and gray areas.

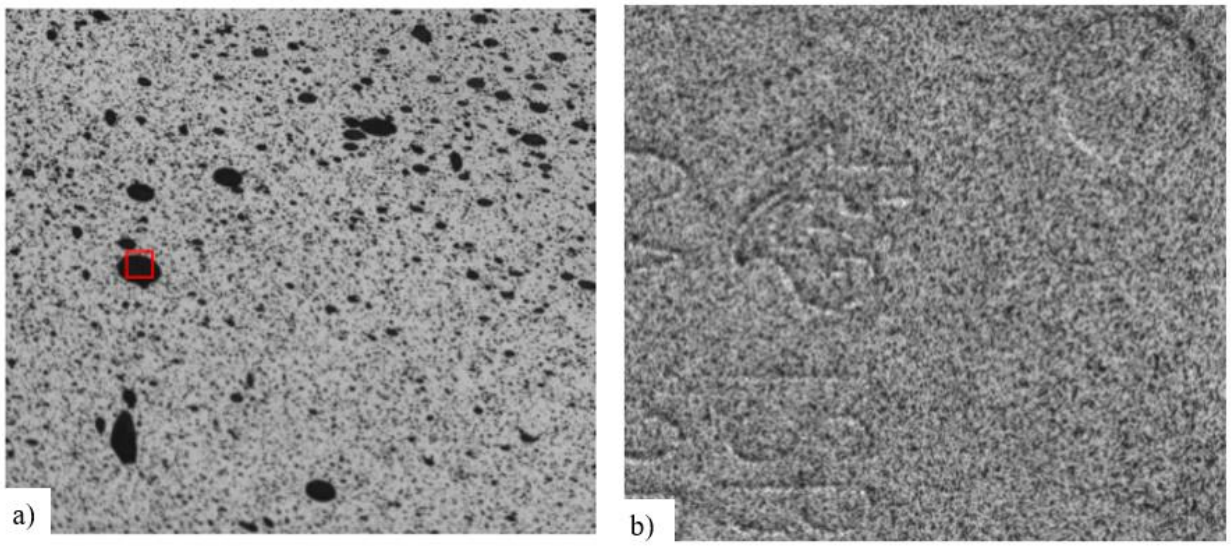


*Figure 14 - **(a)** Pattern that is too large resulting in black areas **(b)** pattern that's too small resulting in aliasing [25]*

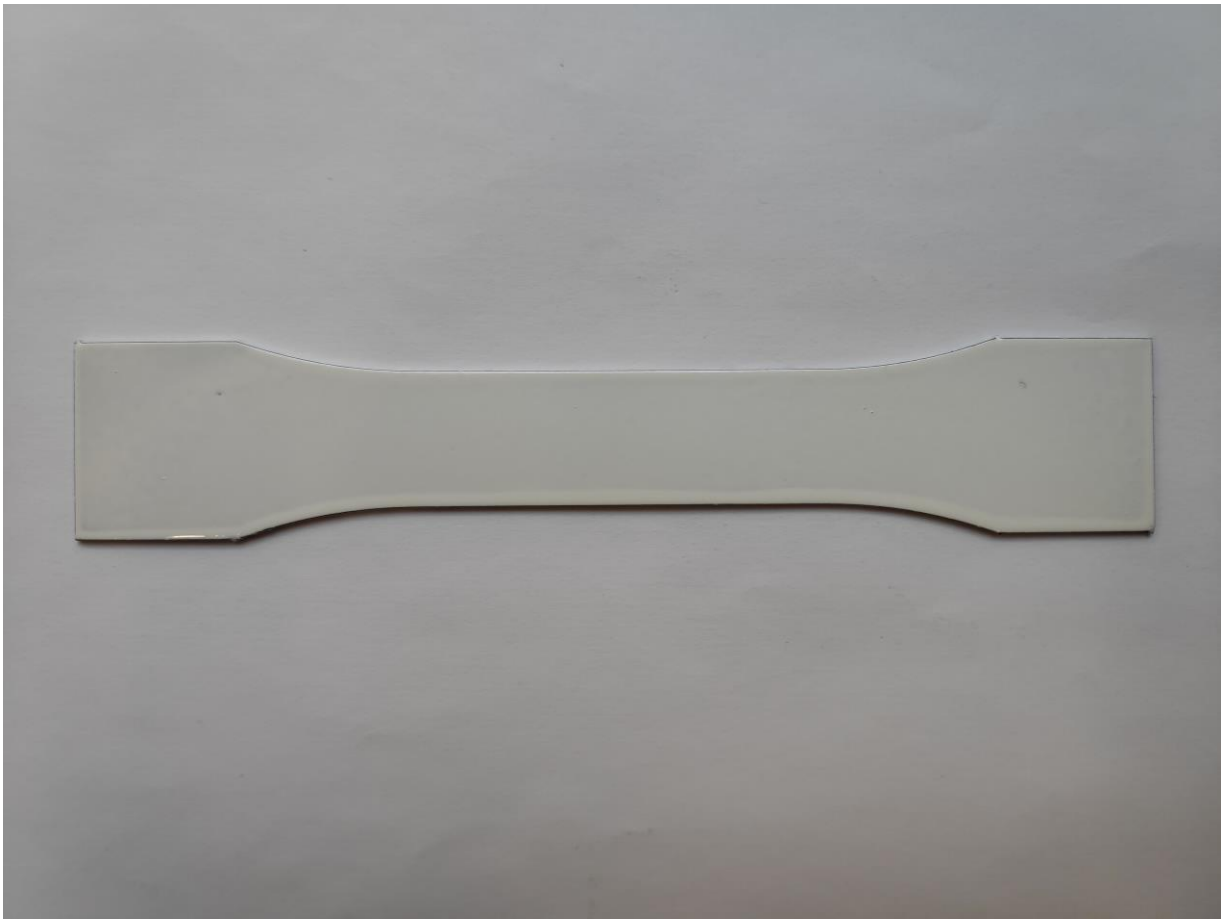

*Figure 15 - Painted specimen*

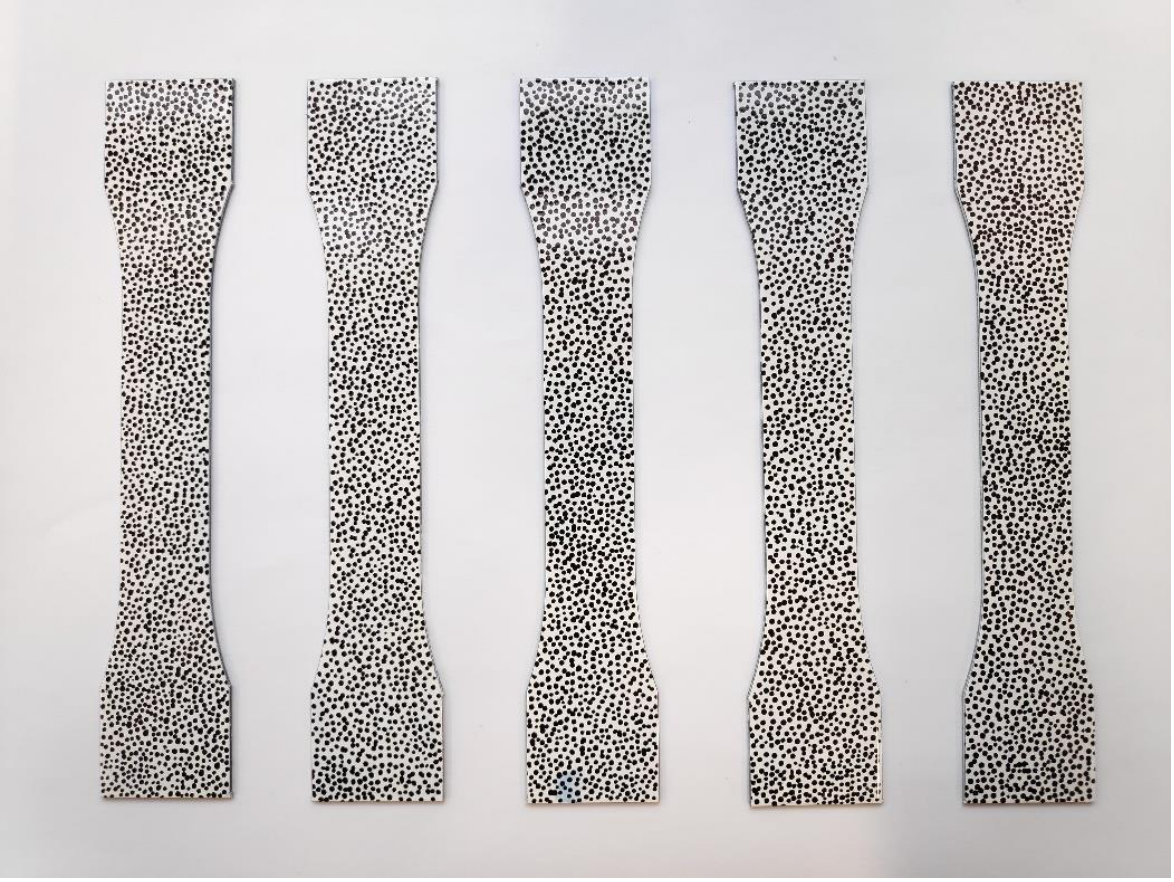

*Figure 16 - Specimens with paint and speckle pattern applied*

With all sixteen specimens prepared for testing, 3D DIC was conducted in conjunction with the uniaxial testing for the different specimens tested. Images were captured at a rate of 2 images per second using a Correlated Solutions' Vic-Snap software and subsequently correlated using Correlated Solutions' Vic-3D 9 software. A total of 16 tests, 4 tests per thickness, were conducted one after the other while maintaining the same DIC tripod position, shutter speed, lens diaphragm settings, and room lighting conditions. Moreover, a single set of calibration was performed for each of the four sets to ensure consistency in the results and remove any DIC experimental bias. Figure 17 shows an annotated photograph of the experimental setup highlighting the main components of the test. The universal testing machine (UTM) was programmed to perform a

displacement-driven tensile test at a crosshead speed $\dot{\delta} = 0.5\, mm/min$ until failure. The same cross-head speed was used for all 16 tests so as to isolate the geometry effects of the structure's thickness. The deformation rate though is indeed a parameter that has an effect on the Lüders phenomena as shown in various studies in literature, e.g. [26]. All uniaxial tensions tests were performed at room temperature and the selected cross-head speed was well within the ASTM E8/E8M standard [22]. The applied crosshead speed and corresponding tensile loads were recorded at a sampling rate of 10 Hz. A summary of the experimental conditions and parameters is shown in Table 2.

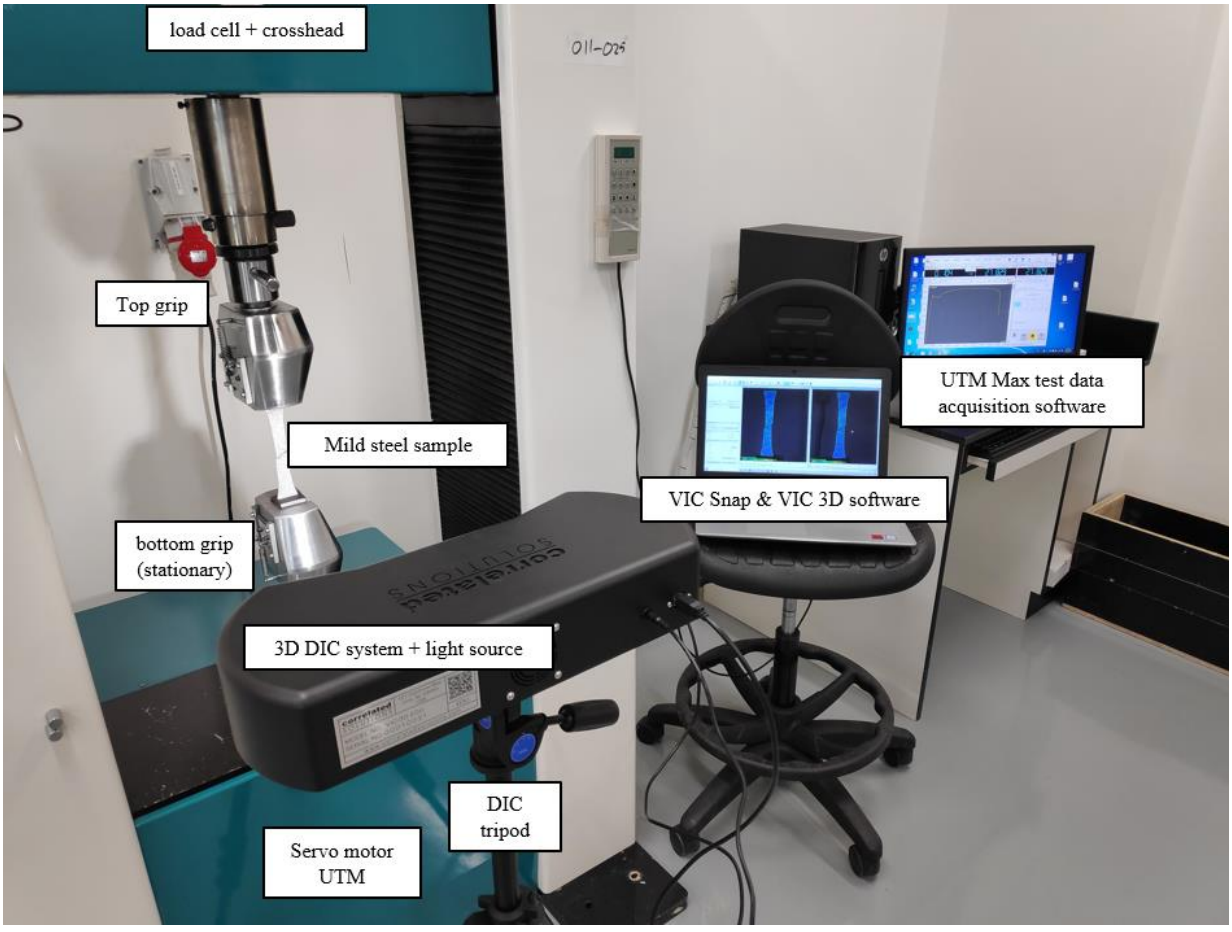


*Figure 17 - Experimental setup: UTM with DIC system, live DIC camera feed, live UTM data*

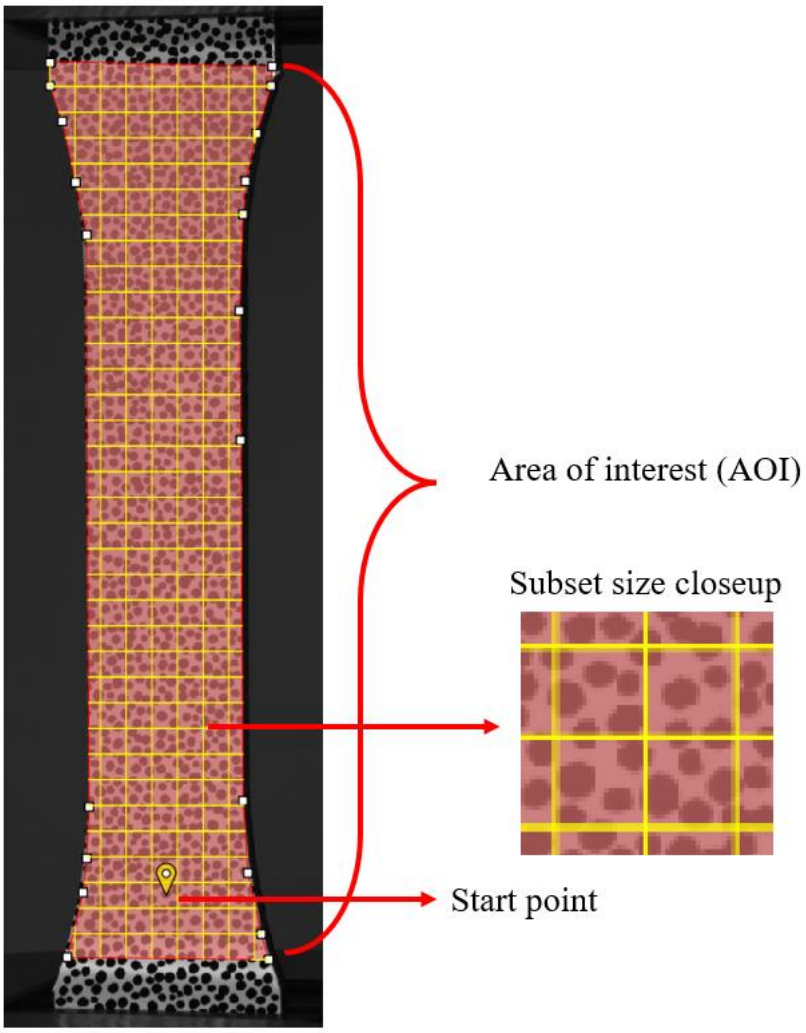


*Figure 18 - VIC-3D settings showing area of interest (AOI), closeup of step size, and starting point of computation*

**Table 2.** Summary of experimental conditions and parameters

| Test number (#) | Thickness (mm) | Loading rate (mm/min) | Frame rate (Hz) | Temperature (˚C) |
|---|---|---|---|---|
| 1 | 1 | 0.5 | 2 | 24 |
| 2 | 1 | 0.5 | 2 | 24 |
| 3 | 1 | 0.5 | 2 | 24 |
| 4 | 1 | 0.5 | 2 | 24 |
| 5 | 2 | 0.5 | 2 | 24 |
| 6 | 2 | 0.5 | 2 | 24 |
| 7 | 2 | 0.5 | 2 | 24 |
| 8 | 2 | 0.5 | 2 | 24 |
| 9 | 3 | 0.5 | 2 | 24 |
| 10 | 3 | 0.5 | 2 | 24 |
| 11 | 3 | 0.5 | 2 | 24 |
| 12 | 3 | 0.5 | 2 | 24 |
| 13 | 4 | 0.5 | 2 | 24 |
| 14 | 4 | 0.5 | 2 | 24 |
| 15 | 4 | 0.5 | 2 | 24 |
| 16 | 4 | 0.5 | 2 | 24 |

As noted earlier, the quality of the speckle patterns on all 16 samples were almost identical, which conveniently allowed for using the same digital image correlation parameters: namely a step size of 7 and subset size of 27 as shown in Figure 18. The subset should be adequately sized to contain enough information of distinguish it from surrounding areas. According to the Vic-3D Manual, a

good subset size has approximately four to five speckles in the frame [23]. The step size controls how many pixels apart each data point is, whereby a good default is to use a step size of ¼ of the size of the subset [23]. This further helped remove any experimental bias when analyzing all 16 sets of results and comparing the Lüders band with respect to the different thicknesses. The reference points were all chosen at the very bottom of the area of interest (AOI) where the subsets experienced the least deformations as the lower grip of the UTM used is stationary. This reference point is a start point from where the Vic-3D software will start looking for initial guesses in the background. It is good practice to place this reference point in the area of the image that undergoes the least amount of motion during the test [23]. In this setup, the lower grip of the UTM is stationary and is therefore the most appropriate location.

# Chapter 3. Results & Discussions

The UTM data obtained was exported to MATLAB for further analysis. Figure 20 to Figure 23 show the combined stress-strain curves for a sample of each of the thickness sets, with a magnified view of the Lüders effect (sharp yield point and subsequent yield plateau). Important to note is that DIC strain data were used instead of crosshead displacement data. This was done to provide more accurate and reliable strain values. In literature, DIC measurements have been shown to provide accurate strain data comparable to physical extensometers and strain gages. Figure 19 illustrates a sample of the vertical strain correlated results obtained from testing.

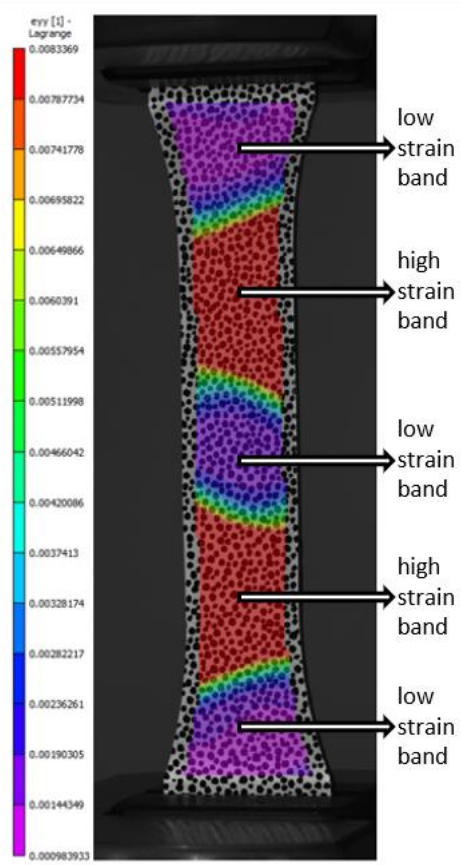


*Figure 19 - DIC vertical strain data*

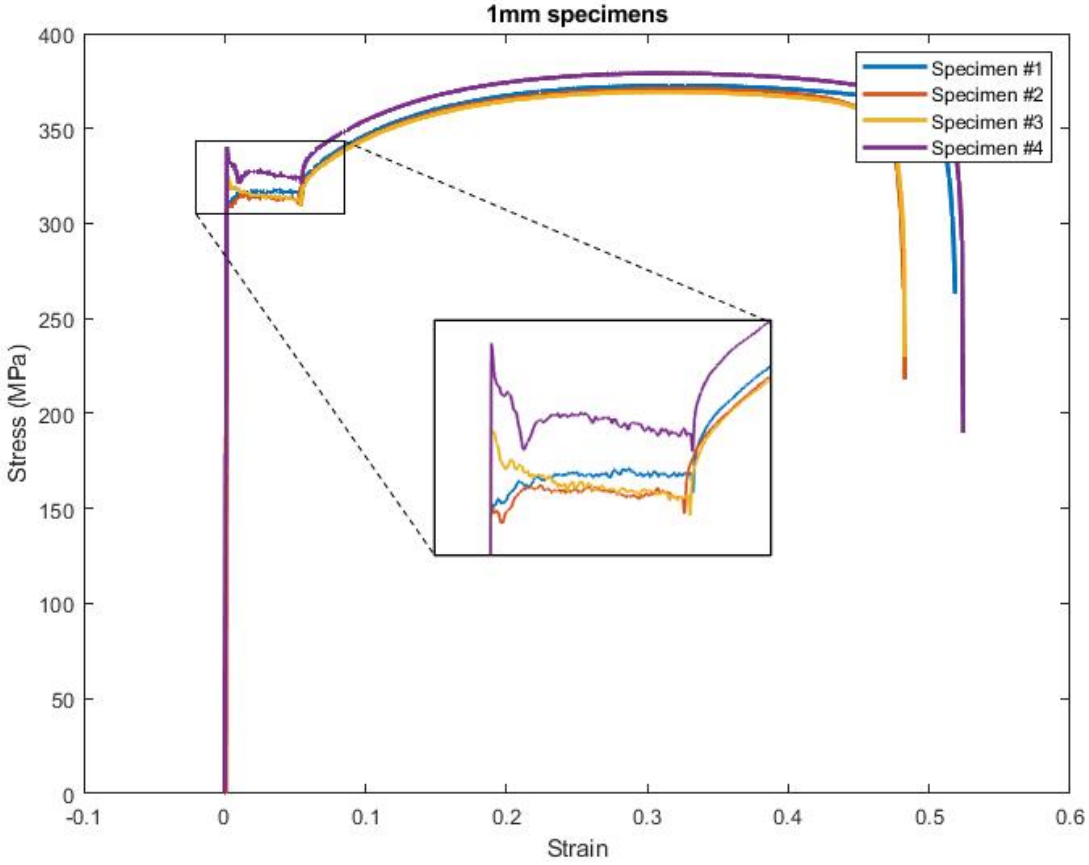


*Figure 20 - Stress-strain curves for four specimens of 1 mm thickness*

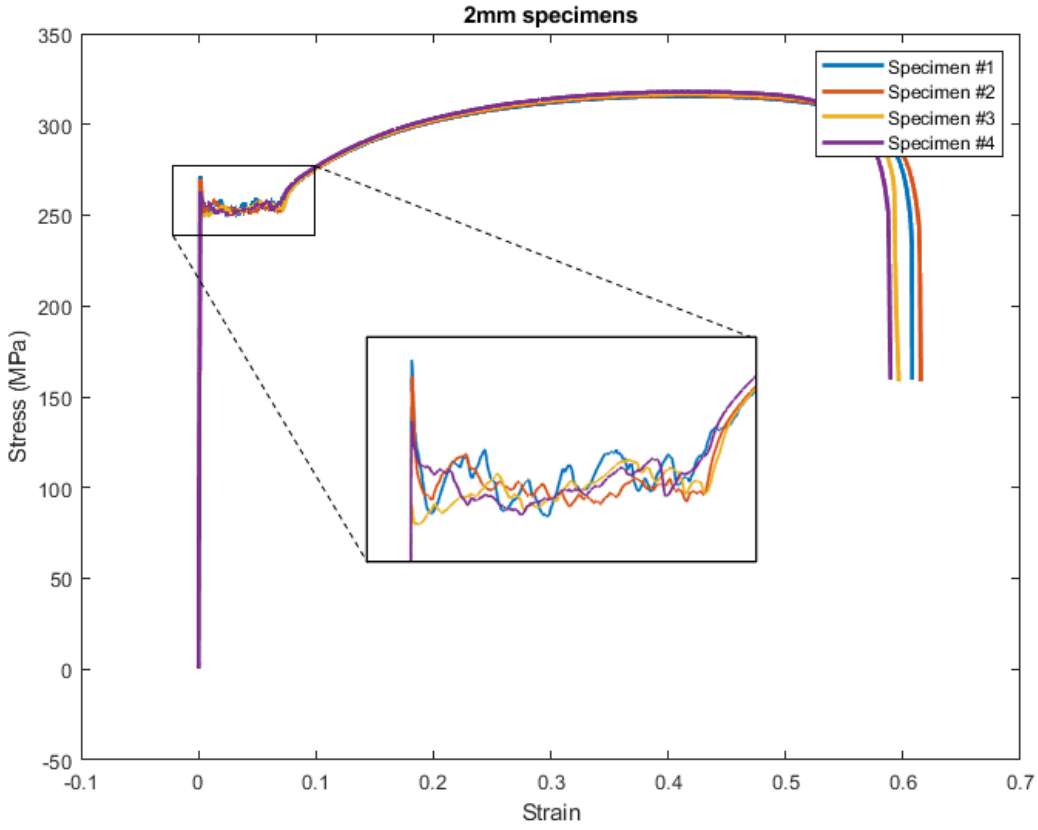


*Figure 21 - Stress-strain curves for four specimens of 2 mm thickness*

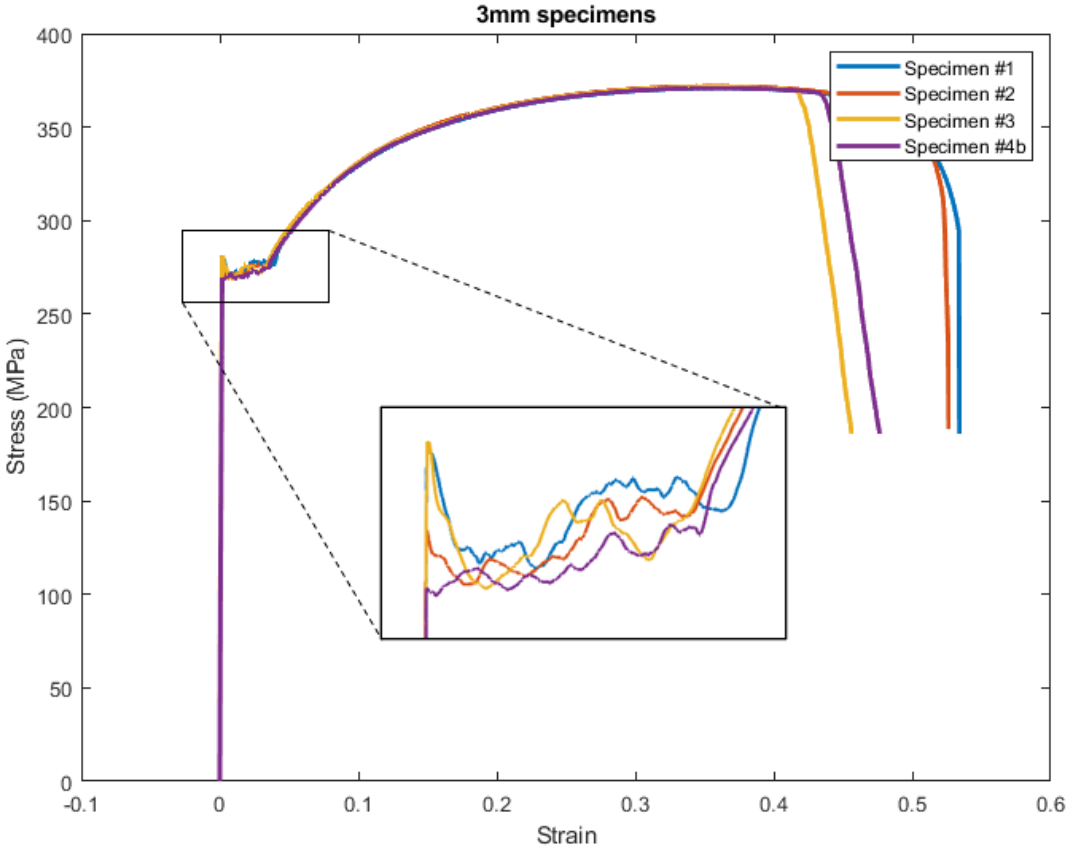


*Figure 22 - Stress-strain curves for four specimens of 3 mm thickness*

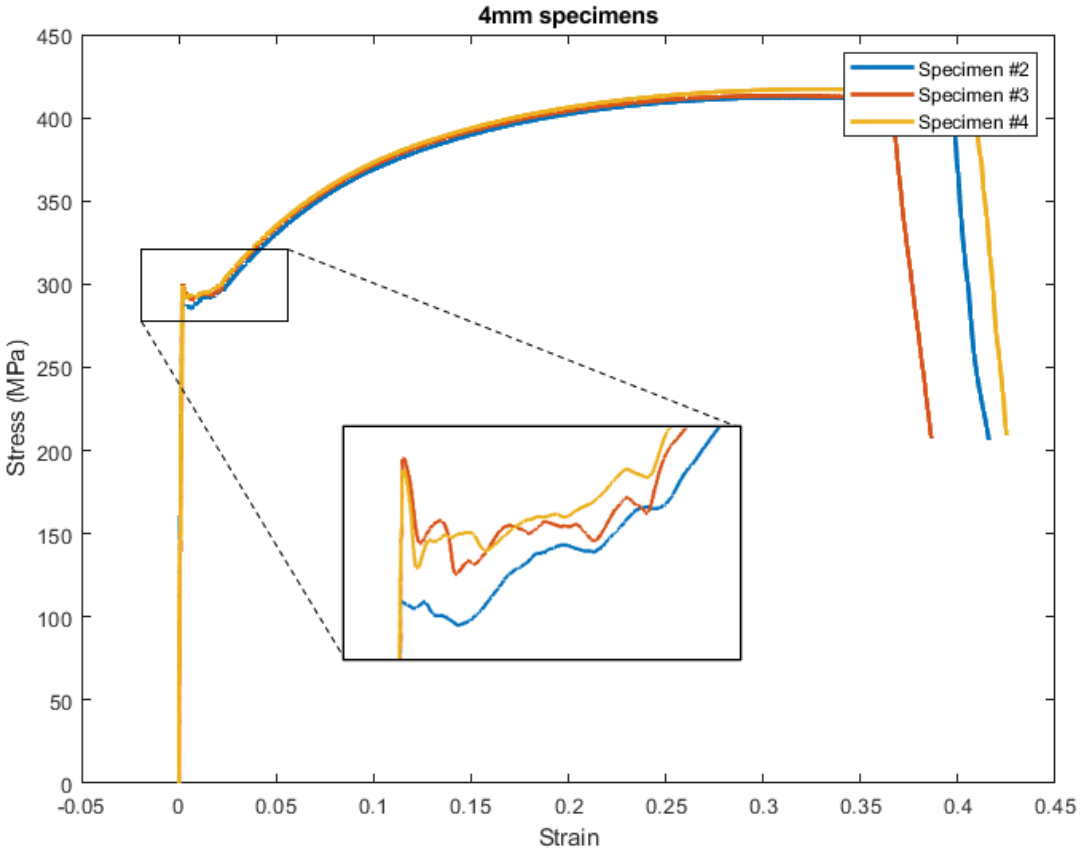


*Figure 23 - Stress-strain curves for four specimens of 4 mm thickness*

Figure 24 plots the load-deflection curves for all the tests conducted with data obtained from the UTM crosshead reading, demonstrating a great level of repeatability. It's important to note that DIC strain data was used instead of crosshead displacement date in the analysis to follow. This was done to provide more accurate strain values. Note that test #16 is not shown due to an error in retrieving UTM data for that particular test. Initial observations reveal that the Lüders deformation phenomenon was observed on all AIS 1524 steel specimens, indicating a material instability during the elastic to plastic transition. However, not all samples exhibited an upper yield stress (UYS)

prior to the stress plateau at the lower yield stress (LYS) point. More specifically, the 1 mm samples revealed little to no drop in the stress level at the onset of the Lüders plateau. A close up on of the stress-strain curve for test #1 (1 mm thickness) is shown in Figure 25. Whereas tests #5 through #15 for the 2 mm, 3 mm and 4 mm thick samples, did exhibit a clear UYS before it drops and settles at the plateau level of the LYS. On a microstructural level, the UYP corresponds to unlocking of the dislocations caused by breaking from impurity atmospheres in the vicinity of stress concentrators [5]. The LYS corresponds to the movement of grains caused by the dislocations, accumulating in a group of yielded grains. The stress plateau in the stress-strain curve reflects the propagation process, for which this study is investigating at the macrostructural level.

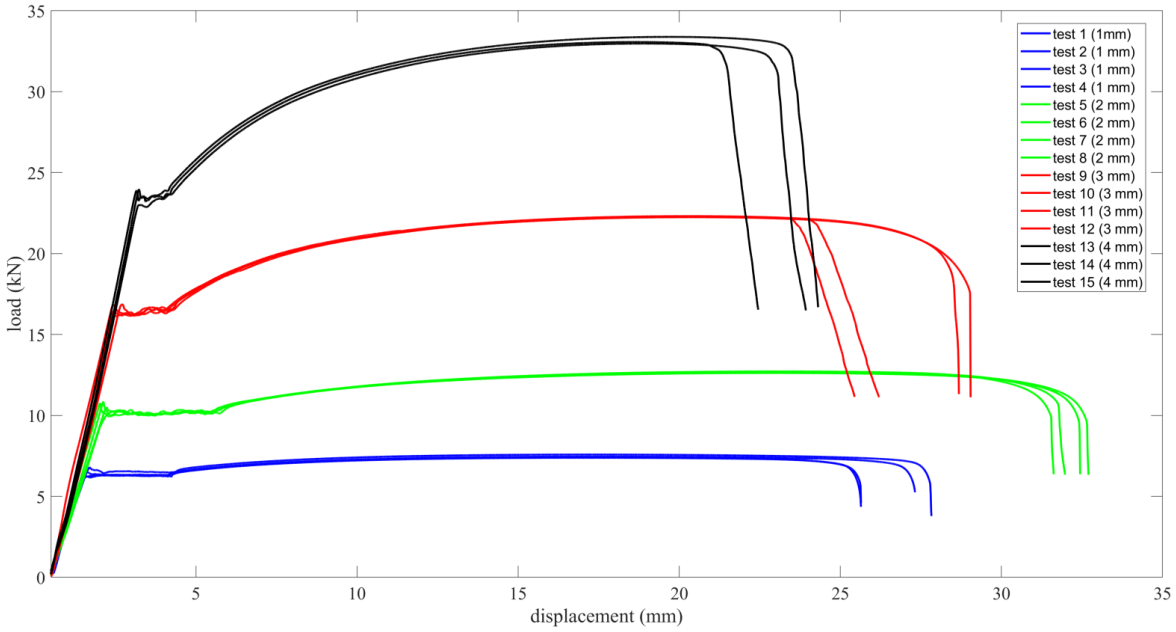


*Figure 24 - Combined load-displacement curves for all samples in Table 2*

Although the primary focus of this work is on a macrostructural level, on a microstructural level the Lüders effect can be explained by looking into pre-yield microstrain that is caused by breaking of dislocations from impurity atmospheres in the areas surrounding large concentrations of stress [5]. This, in turn, accumulates to a large cluster of dislocation around the grain boundaries. With increasing tensile stress, these dislocations cause neighboring grains to shift, thereby producing a pileup of yielded grains, which results in the formation of Lüders bands we observe in the following sections.

With the objective in this work focused on investigating Lüders phenomena in AISI 1524 steel, the following subsections will focus on quantifying the different Lüders band. Section 3.1 – Lüders band initiation, Section 3.2 – Lüders strain ($\Delta\varepsilon_L$), Section 3.3 – the Lüders band width ($w_{band}$), Section 3.4 – the Lüders band propagation velocity ($v_{band}$) and Section 3.5 – The Lüders band spatial features highlighting the number of band formations and their locations, in addition to the angle the band's front forms with respect to the vertical tension direction ($\theta_{band}$).

## *3.1. Lüders Band Initiation*

In the work presented here the Lüders strain initiation was identified by observing the vertical tensile strain DIC data. This is the most prevalent and reliable metric to identify the band's nucleation. Strain rate data is also shown in literature to be useful for such identification, e.g. [27] [28]. For all AISI 1524 samples tested, it was observed that the Lüders band starts to nucleate ahead of the UYS regardless of the sample's thickness. Figure 26 reveals an example of the band evolution at the very early stages of the Lüders phenomena, where six frames were chosen in the

neighborhood of the yield as shown in the corresponding locations of the frames on the stress strain curve of Figure 25. More specifically, frames #358 and #364 occur just before the yield point, yet high strain peaks (i.e. Lüders band nucleation) are observed to start to form on the opposite ends of the specimen as indicated by the arrows in frames #358 and #364 of Figure 26. It was also found that the Lüders band for AISI 1524 steel forms in a very short time. For instance, the formation process of the top band took only a duration of 15 seconds for this particular sample thickness of 1 mm. Similar results are found in the specimens of different thickness, as shown in Figure 27 to Figure 29.

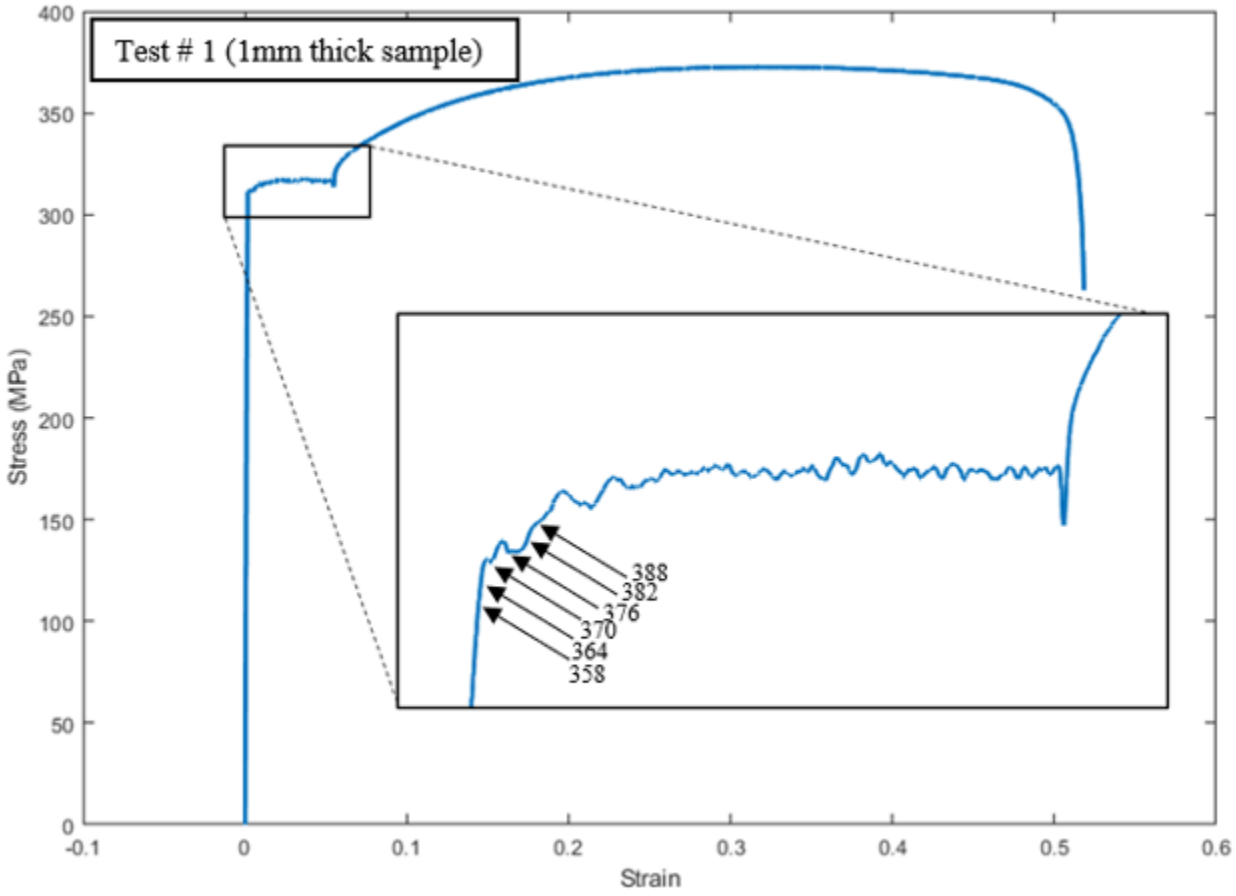


*Figure 25 - Stress strain curve for test #1 (1 mm thickness) showing nucleation of the Lüders band*

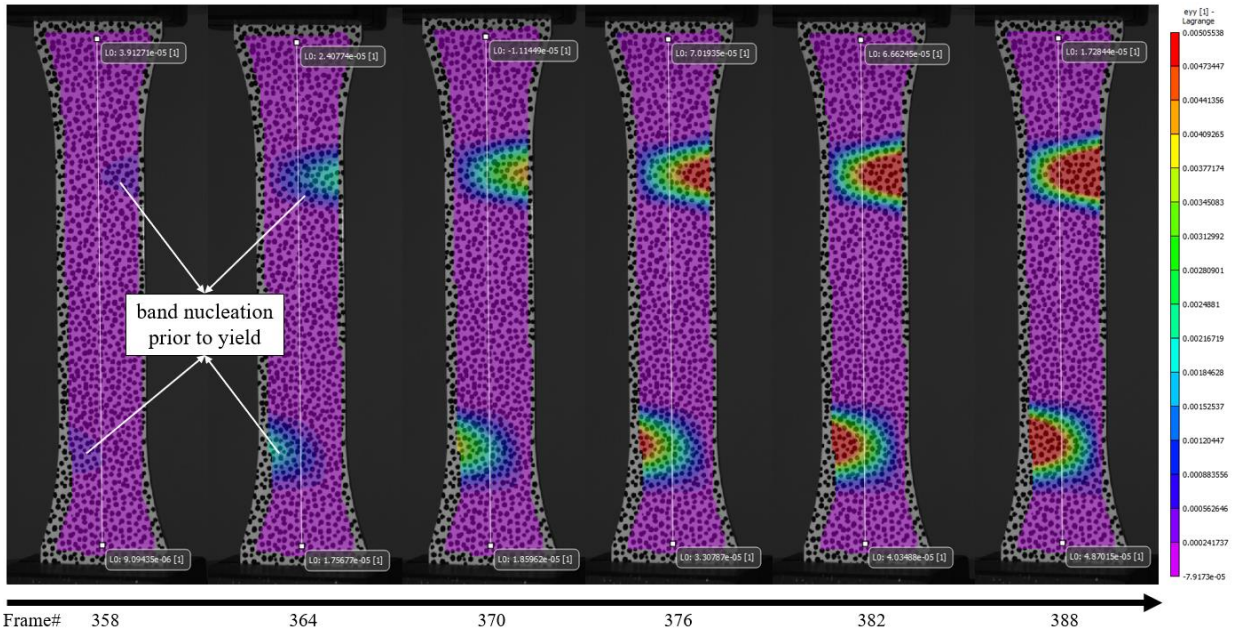


*Figure 26 - DIC $\varepsilon_y$ at 5 frames in the vicinity of yield point Stress strain curve for test #1 (1 mm thickness) showing nucleation of the Lüders band*

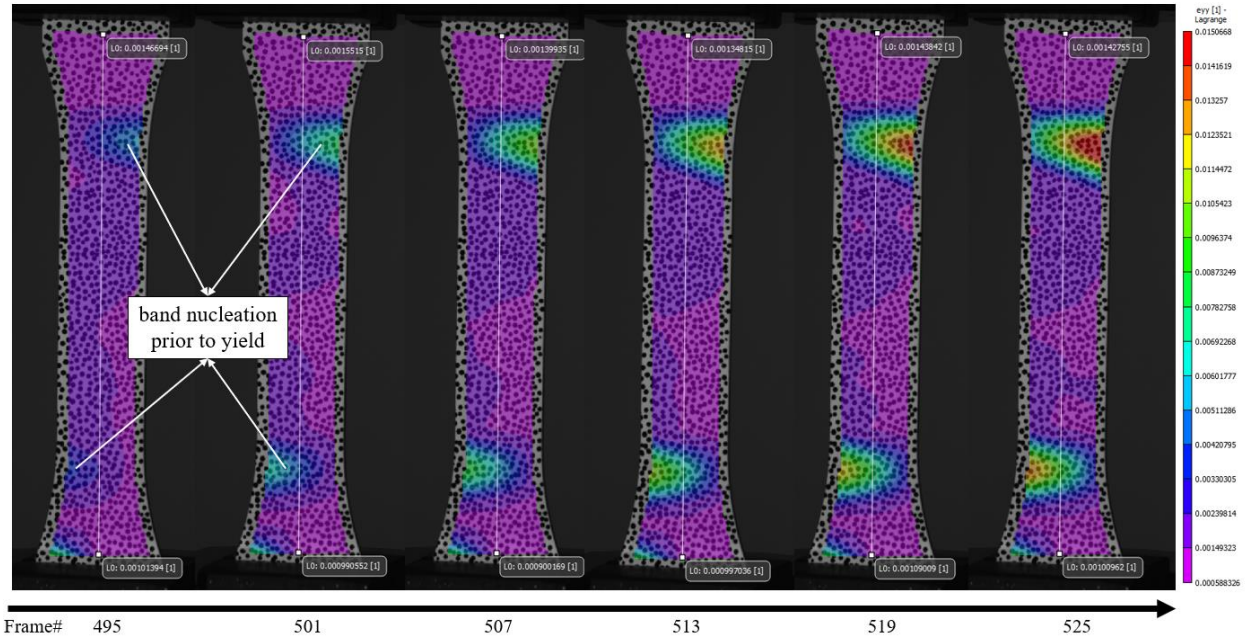


*Figure 27 - DIC εy at 5 frames in the vicinity of yield point Stress strain curve for test #2 (2 mm thickness) showing nucleation of the Lüders band*

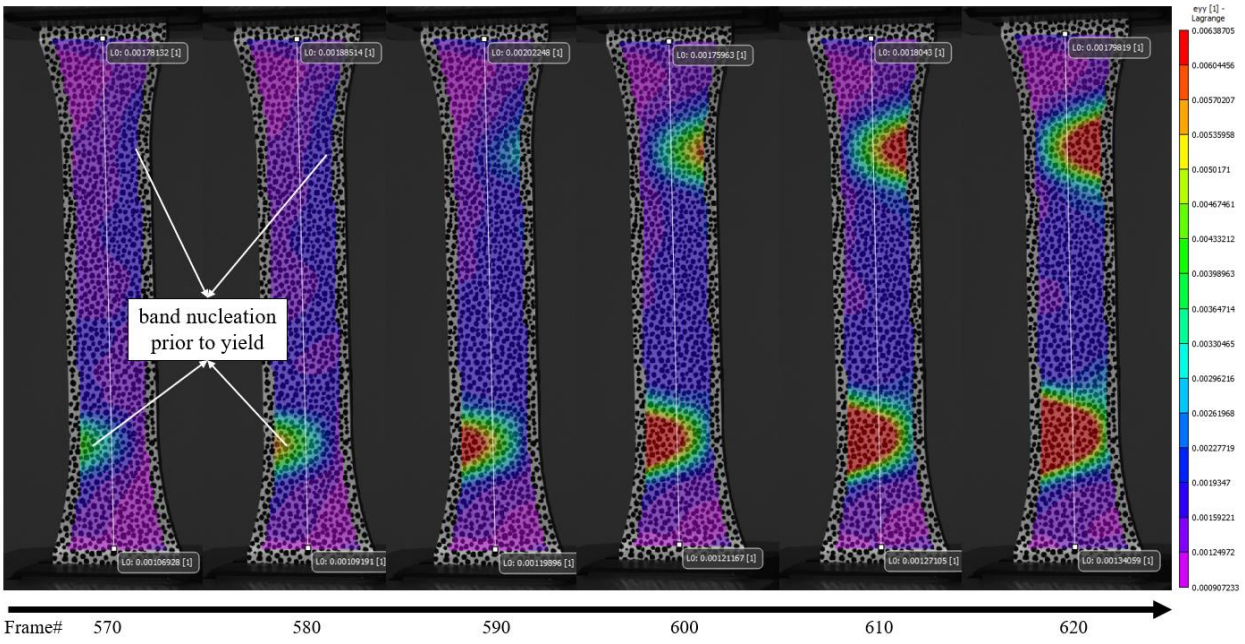


*Figure 28 - DIC εy at 5 frames in the vicinity of yield point Stress strain curve for test #2 (3 mm thickness) showing nucleation of the Lüders band*

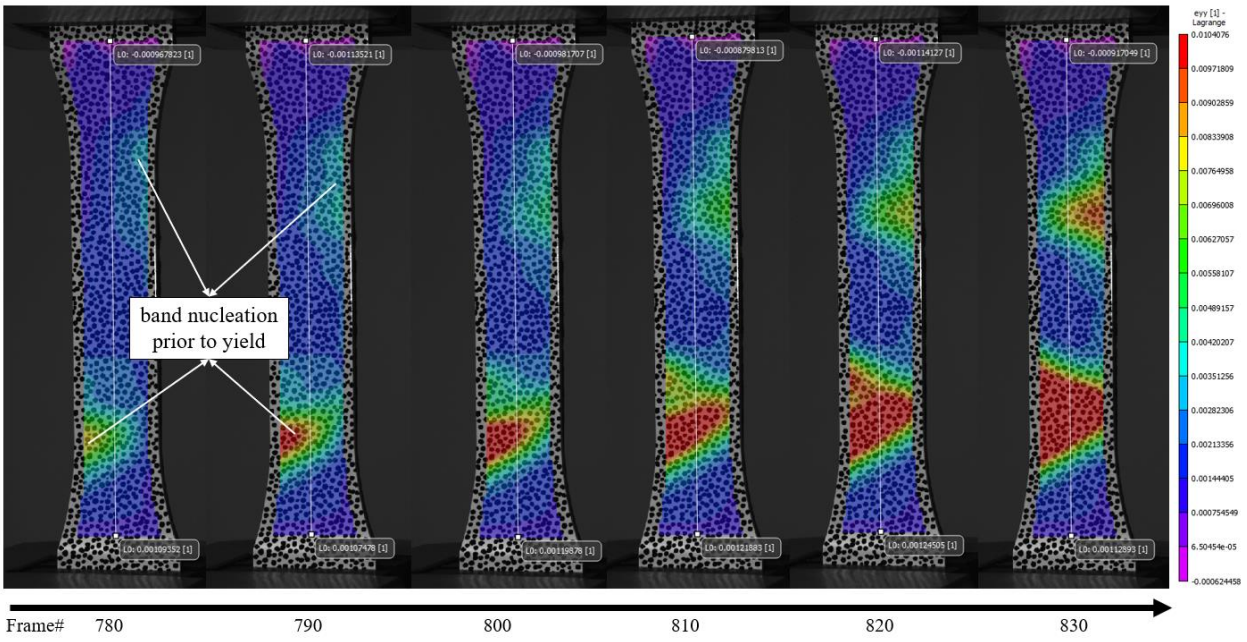


*Figure 29 - DIC εy at 5 frames in the vicinity of yield point Stress strain curve for test #2 (4 mm thickness) showing nucleation of the Lüders band*

While the macroscopic stress concentration can be induced by the microstructure heterogeneity or geometry change of the specimen, the Lüders band nucleation was observed at the top right corner and the bottom left corner in almost all tested samples. This can be attributed here to the gripping process where some torques (i.e. twist) were induced on the samples upon gripping that were very likely to have primed the strain concentrations to occur at such locations.

## *3.2. Lüders Strain*

An initial observation here is that the Lüders plateau region decreases (in duration along the strain axis) with increasing sample thickness. This plateau region is often referred to as the Lüders strain, $\Delta\varepsilon_L$. More specifically, the elastic regime terminates abruptly at the UYS, where the stress drops down to a plateau at the LYS that extends over a strain $\Delta\varepsilon_L$. The averaged $\Delta\varepsilon_L$ from all tests conducted in Table 2 were observed to be 4.3% for the 1 mm thick samples, 6.4% for 2 mm samples, 2.7% for 3 mm samples and 1.8% for 4 mm samples. Interestingly, the 2 mm thick

samples exhibited a slightly larger Lüders strain (i.e. a more elongated plateau region) that then 1 mm thick samples as seen in Figure 5. Though the more pronounced trend can be seen in the decrease in the Lüders strain with the 3 mm and 4 mm thick samples respectively. The decreasing Lüders strain with increasing material thickness was also observed in work by Cai et al. [7] that investigated a similar thickness effect on 54546 Aluminum alloy.

Figure 30 to Figure 33 show the DIC images of the vertical tensile strain half way through the Lüders plateau region for all 4 thicknesses along with their stress strain curves, with a magnified view of the Lüders effect (sharp yield point and subsequent yield plateau). While Figure 30 to Figure 33 show the results of 4 samples for each thickness level, this was done for all samples listed in Table 2.

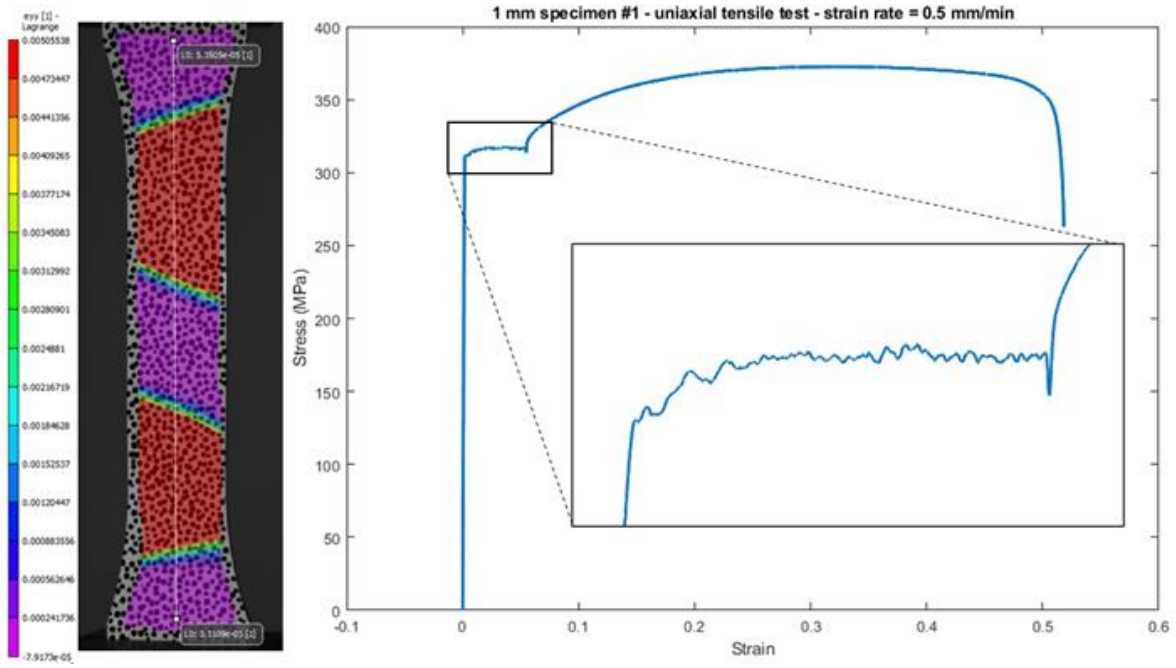


*Figure 30 - Vertical strain data from DIC (left) with respective stress-strain curve (right) for a 1 mm specimen*

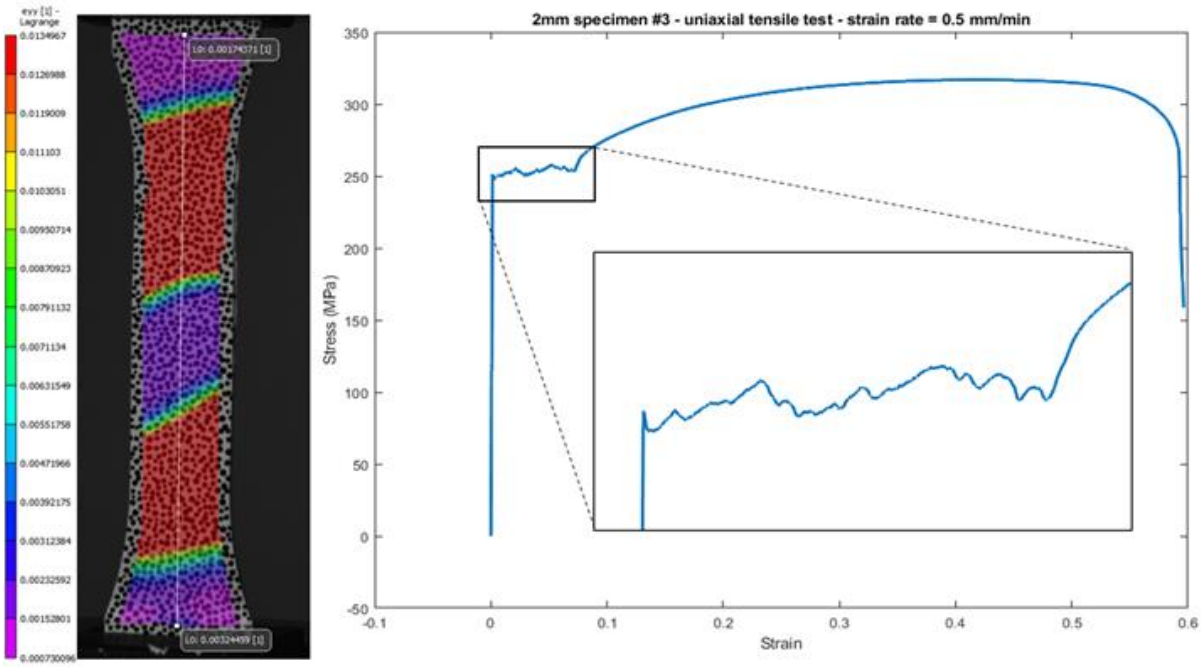


*Figure 31 - Vertical strain data from DIC (left) with respective stress-strain curve (right) for a 2 mm specimen*

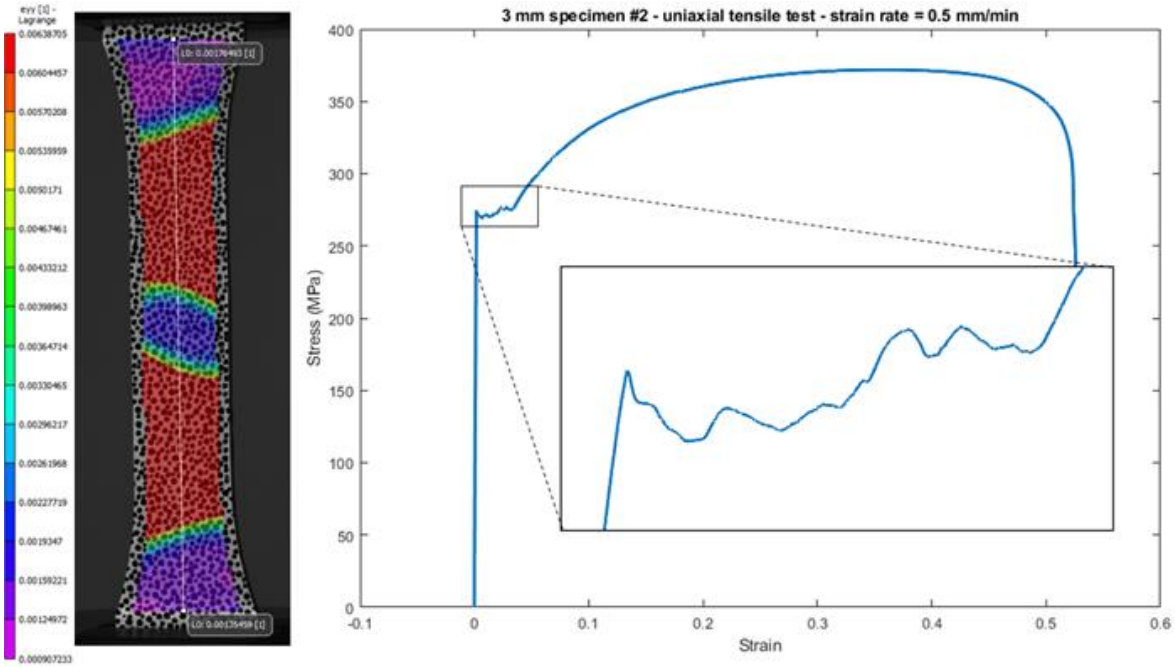


*Figure 32 - Vertical strain data from DIC (left) with respective stress-strain curve (right) for a 3 mm specimen*

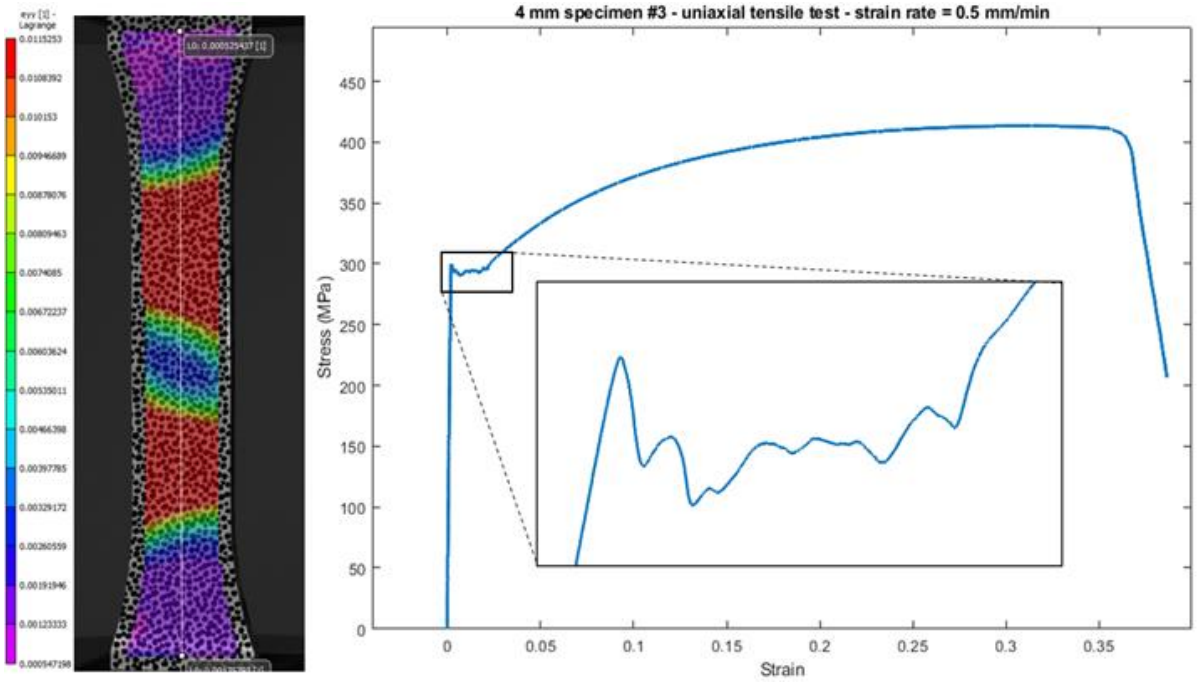


*Figure 33 - Vertical strain data from DIC (left) with respective stress-strain curve (right) for a 4 mm specimen*

As mentioned earlier, notice that the 2 mm, 3 mm, and 4 mm thick samples did exhibit an UYS unlike the 1 mm samples as shown in the magnified images of Figure 30 to Figure 33.

On a microstructural level, in steels made up of the same chemical composition, but with a varying microstructure, the observed Lüders strain is highest when the microstructure is tempered martensite. The lowest Lüders strain, in turn, is observed in materials with a ferrite-pearlite or upper bainite microstructure. This is the result of different morphology of carbides in varying microstructures [18]. Since the microstructure was not investigated for all samples, a slight variation in microstructure between the specimens of different thicknesses could explain the variation in Lüders strain between the specimens. This could be further investigated in a study on a microstructural level.

### *3.3. Lüders Band Width*

The width of the Lüders band, $w_{band}$, was quantified in this study as the distance at the mid-height of the localized strain band as shown in Figure 35. The vertical strain distribution along the vertical centerline was obtained from the Vic-3D software for all five frames as shown in Figure 34. More specifically, the tensile strain magnitude is plotted, Figure 35 (b), along the vertical central line, Figure 35 (a), from which $w_{band}$ was determined for both the top band and the bottom band. Various references in literature use a similar method for measuring the Lüders band width such as that of [7]. Other studies in literature use the strain rate data across the length of the sample instead to characterize the band width [27].

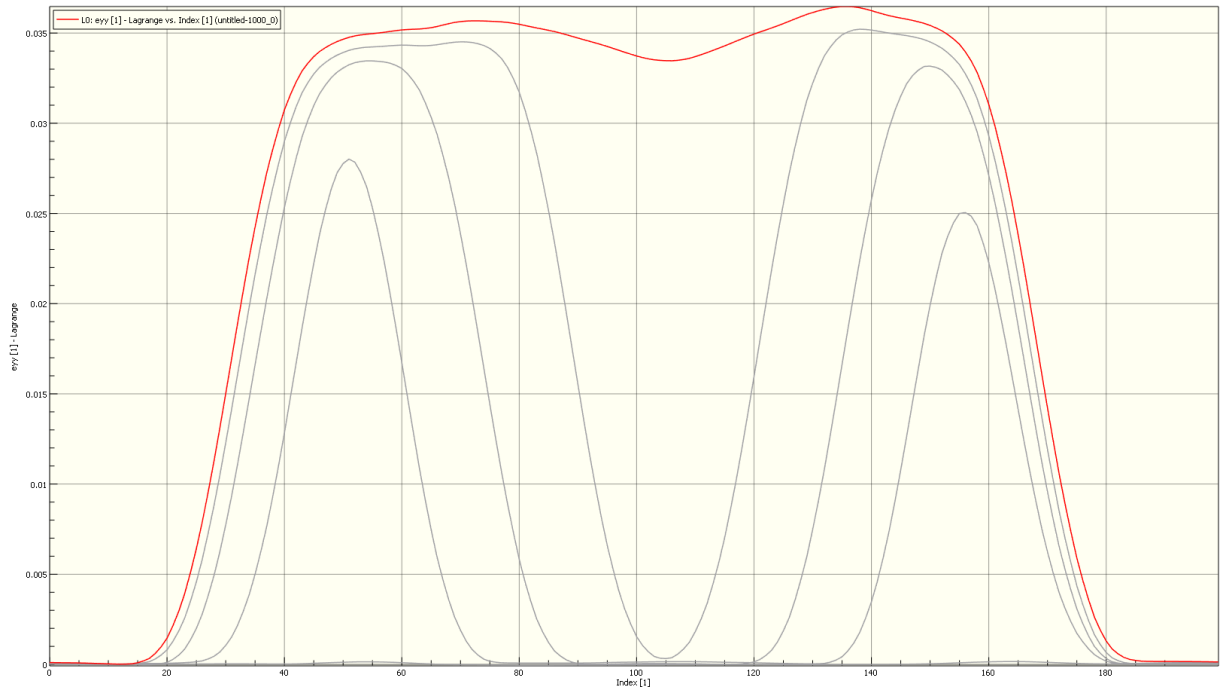


*Figure 34 - Plot of vertical strain distribution along the vertical centerline for five frames*

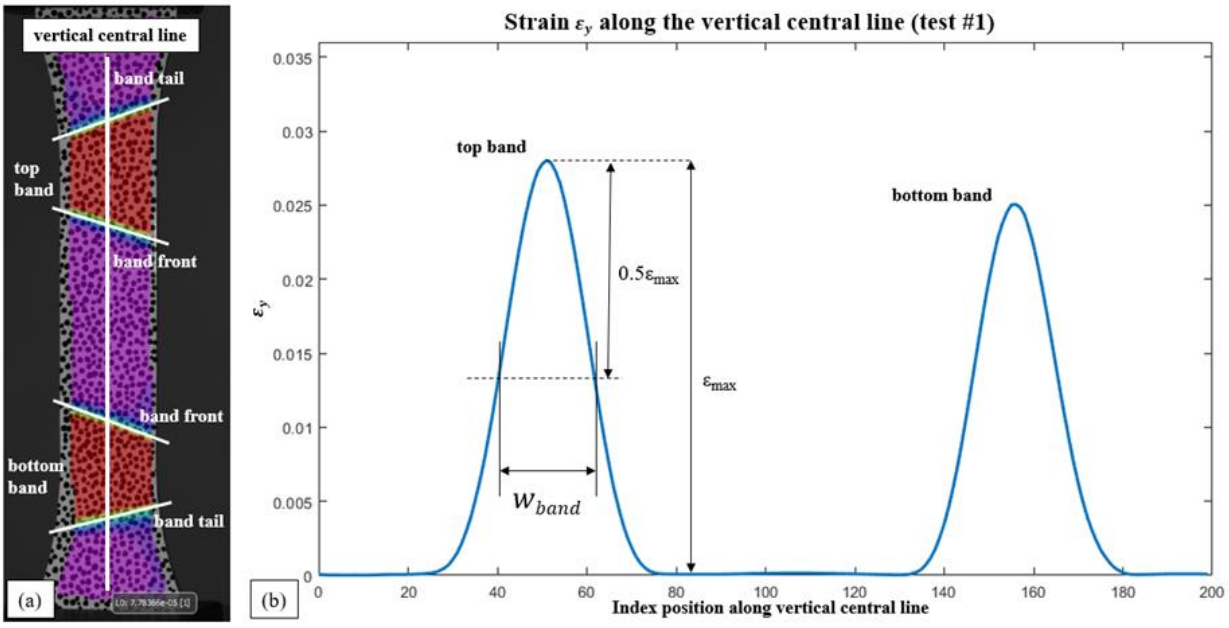


*Figure 35 - Determination of the Lüders band width $w_{band}$ **(a)** Vertical strain data from DIC at frame 25% $\Delta\varepsilon_L$ **(b)** corresponding vertical strain distribution along the vertical centerline*

The band width was analyzed for all samples tested in Table 2. And since $w_{band}$ will be increasing during the course of the Lüders plateau, the width here was calculated for all samples at the point of 25% $\Delta\varepsilon_L$, at which point the Lüders band would have fully developed. The second contour strain plot in Figure 38 (b). For instance reveals the band fully developed at a quarter of the Lüders plateau duration. Furthermore, the band width was analyzed for both Lüders bands; namely the top band, $w_{top}$, and the bottom band, $w_{bottom}$. With all the bands quantified in that manner described in Figure 35, $w_{top}$ and $w_{bottom}$ for the four thicknesses investigated are plotted in Figure 36 (left y-axis). A clear trend was observed in that an increase in AISI 1524 steel thickness resulted in the width of both Lüders bands formed. Similar results are found in literature on other materials, such as aluminum [3]. Moreover, I found that $w_{top}$ was larger than $w_{bottom}$ across all thicknesses. This former conclusion goes along the same lines of the earlier observation that the top band nucleated and formed prior to the bottom one.

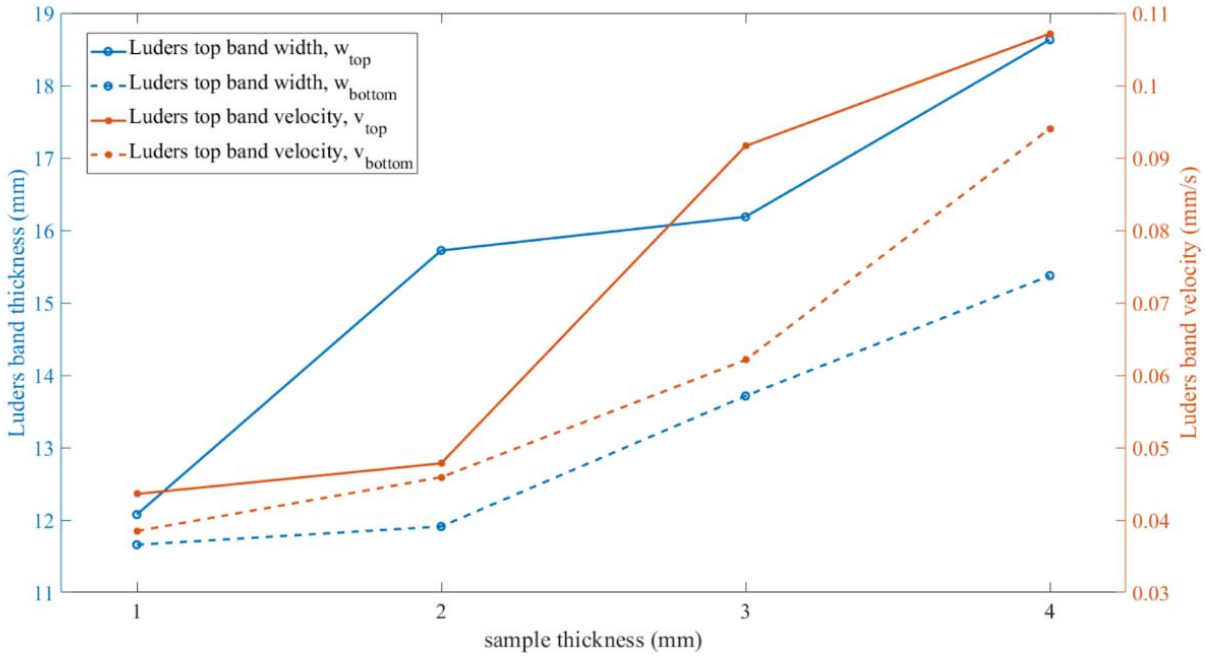


*Figure 36 - Averaged results for the Lüders band thickness (left y-axis) and velocity (right y-axis) at 1 mm, 2 mm, 3 mm and 4 mm thickness*

## *3.4. Lüders Band Velocity*

In order to calculate the band propagation velocity, the change in the band's position along the centerline was tracked over different time intervals (i.e. at different frames) during the course of the Lüders plateau. Figure 37 demonstrates the determination of the Lüders band velocity in the case for test #1. Both the top and bottom band velocities were calculated for all AISI 1524 steel samples in Table 2. The top band of course propagating downwards and the bottom band propagating upwards. It was observed that the top band exhibited a faster propagation compared to the bottom one. This was the case for all 1 mm, 2 mm, 3 mm and 4 mm samples as shown in the averaged results of Figure 36 (right y-axis). The second observation regarding the Lüders band velocity was that the velocity increased with increasing thickness, as shown in Figure 36 (right y-axis). Such increase in velocity was seen for both the upper and lower bands simultaneously.

Figure 38 offers another visual of the both the top and bottom band propagation evolution for test #10 (3mm thickness) highlighting five different frames, at equally spaced intervals, 0% $\Delta\varepsilon_L$, 25% $\Delta\varepsilon_L$, 50% $\Delta\varepsilon_L$, 75% $\Delta\varepsilon_L$ and 100% $\Delta\varepsilon_L$ respectively.

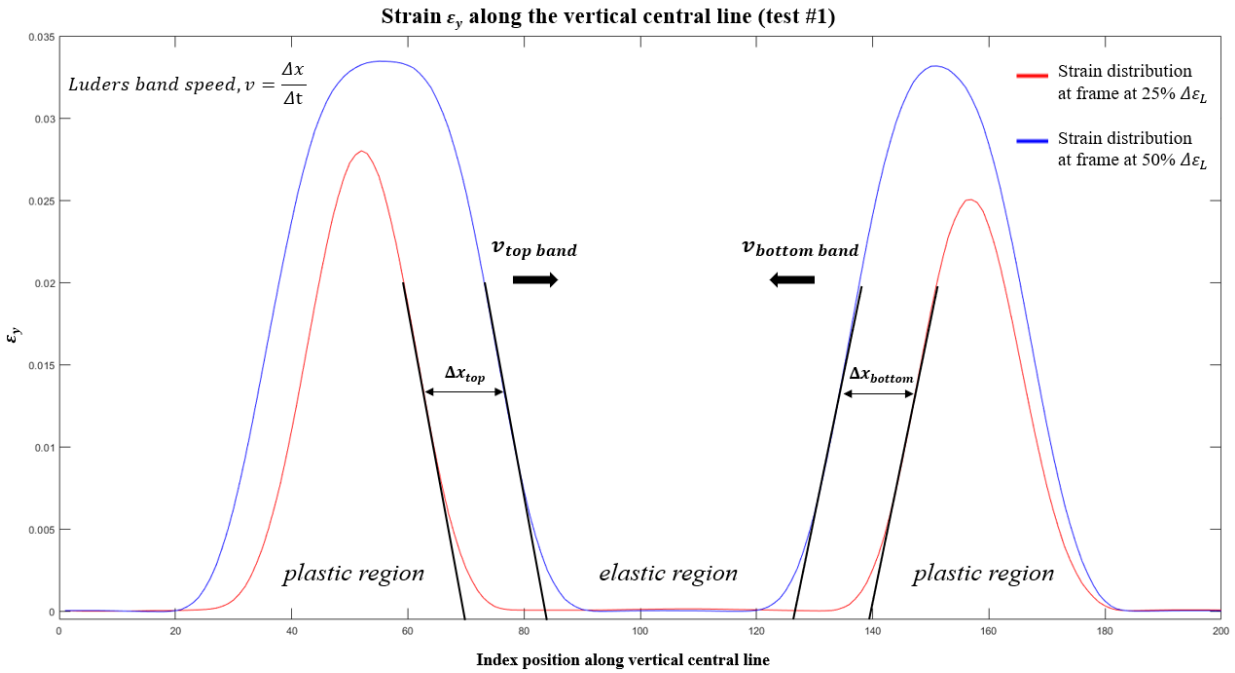


*Figure 37 - Determination of the Lüders propagation speed $v_{band}$ via tracking the band's position over two time intervals (e.g. frame at 25% $\Delta\varepsilon_L$ and frame at 50% $\Delta\varepsilon_L$*

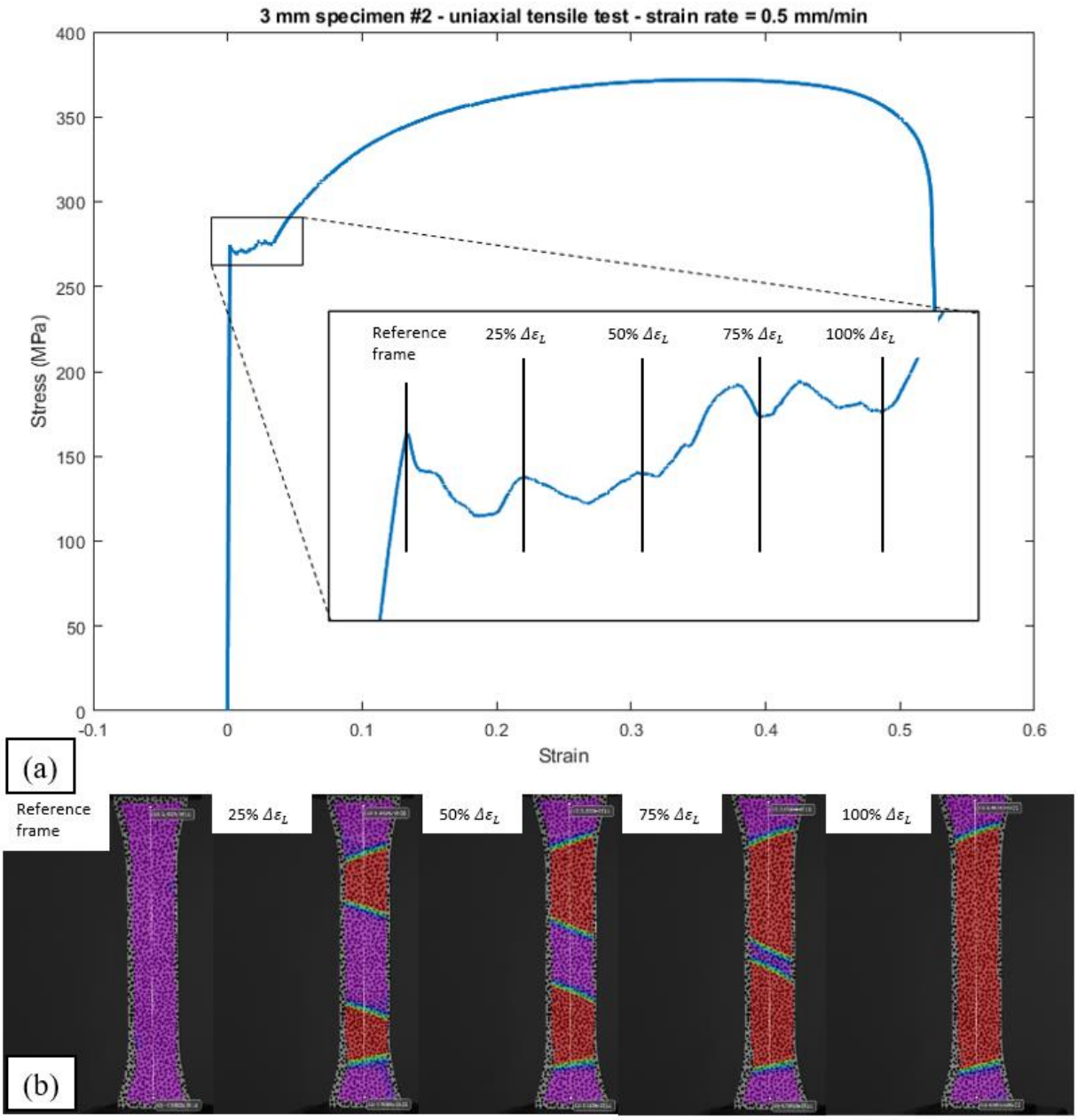


*Figure 38 - Determination of the Lüders band velocity, v_band **(a)** Stress-strain curve of 3mm specimen, highlighting 5 frames within the Lüders band **(b)** Five DIC captures of strain in the Y-direction, showing the propagation of Lüders bands through a 3 mm specimen*

## *3.5. Spatial Features*

For all the samples tested with various thicknesses, the AISI 1524 steel samples exhibited the formation of two simultaneous bands at the very top and very bottom of the sample's flat surface. Examples of those are shown in Figure 30 to Figure 33 for all four thicknesses tested. This is unlike most aluminum alloys, where literature shows the formation of a single Lüders band around the center of the specimen [7]. A single band formation was also observed in the case of nickel titanium alloys [29]. Other literature investigating Lüders strains corroborates the findings presented here that two bands occur in low alloy steels [27] and [30]. Moreover, I observed that the two bands forming on opposite ends of the specimen had complimentary shapes as they propagated towards one another. Using protractor software, these angles were determined as shown in Figure 39. More specifically, the front of the top band and the front of the bottom band had an almost identical angle, $\theta$, in all four thicknesses tested as shown in Figure 40. This in fact is unlike some other experimental results in literature, [27], where the front of the top and bottom bands did not form complimentary matching angles. It is postulated here that the Lüders band nucleation taking place at the opposite corners of the sample (i.e. top right and bottom left) in this current study lead to the angles of the top and bottom bands to be complimentary (i.e. the same).

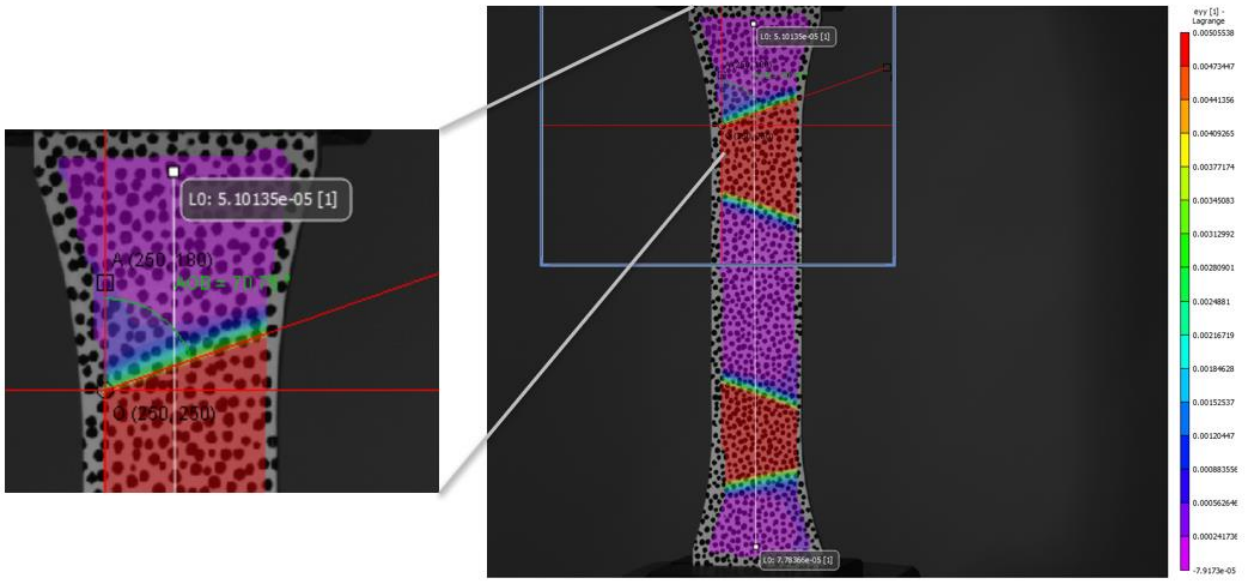


*Figure 39 - Vertical strain data from DIC with overlapping software to measure angle*

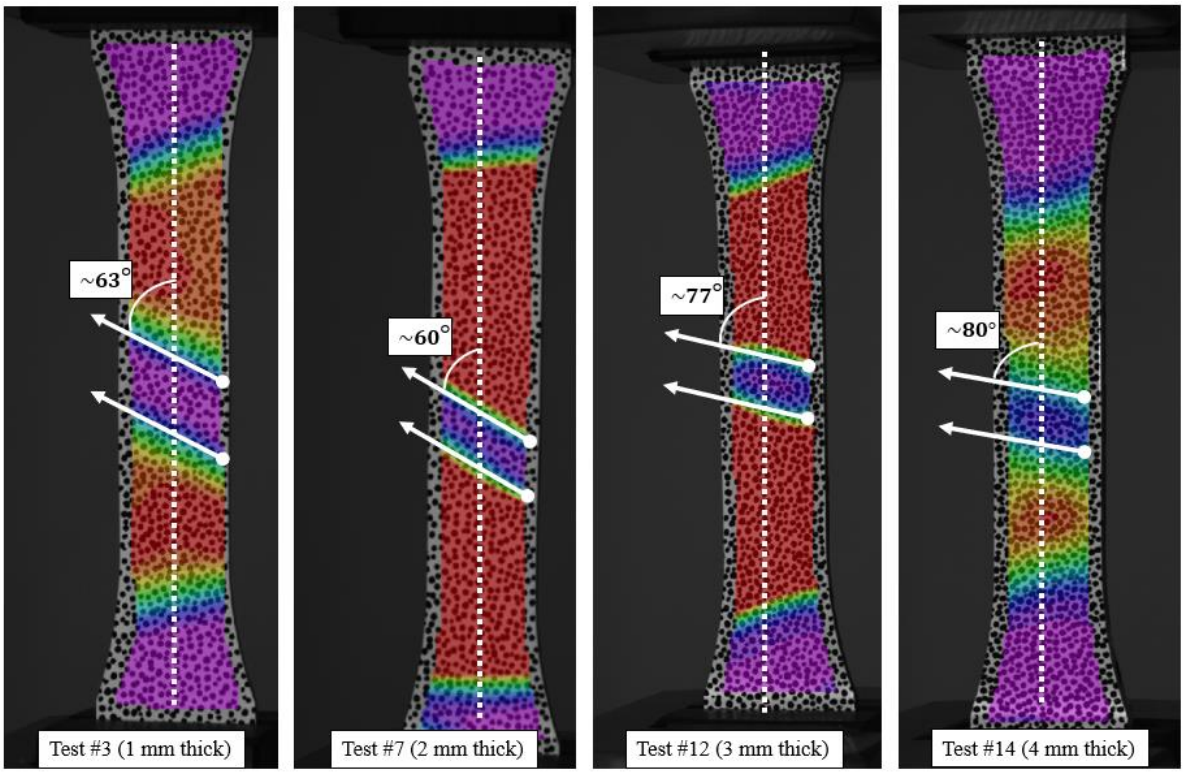


*Figure 40 - Averaged Lüders band inclination with respect to the four thicknesses tested*

Aside from the dual band formation, location at the opposite ends, and complementary shapes, I also found that the localized-deformation region, i.e. the band, lies inclined between 63° and 80° with respect to the vertical tensile direction. While not an evident trend was observed between the 1 mm and the 2 mm samples, I conclude that the angle drops with the increase in thickness, as shown by the trend in and Table 3. This can be attributed to the 3D effect of the Lüders band propagation, whereby the band initiated at the very center of a slender structure and propagates outwards towards the structure's surface before propagating in the tensile direction. In other words, the Lüders band in AISI 1524 steel alloy nucleates at the core of the material and propagates in the thickness direction towards the surface prior to its propagation in the tensile direction.

**Table 3.** Angle between Lüders band and vertical axis at the start of the plateau

| Thickness | Location | Sample 1 | Sample 2 | Sample 3 | Sample 4 |
|---|---|---|---|---|---|
| 1 mm | top band 1 | 71° | 76° | 75° | 85° |
| 1 mm | bottom band 2 | 77° | 73° | 85° | 80° |
| 2 mm | top band 1 | 89° | 74° | 80° | - |
| 2 mm | bottom band 2 | 91° | 83° | 89° | - |
| 3 mm | top band 1 | 80° | 65° | 74° | 71° |
| 3 mm | bottom band 2 | 77° | 72° | 79° | 70° |
| 4 mm | top band 1 | 63° | 79° | 75° | - |
| 4 mm | bottom band 2 | 61° | 71° | 68° | - |

# Chapter 4. Conclusions & Future Work

I performed full-field observations of the Lüders phenomena on commercial mild steel samples focusing on thickness effects. The following points were concluded for AISI 1524 steel alloy regarding the influence of thickness on the Lüders phenomena:

- The Lüders band nucleates ahead of the yield point.
- The Lüders band nucleates at the core of the material and propagates to the surface prior to its propagation in the longitudinal direction
- Lüders strain decreases with increasing thickness.
- Lüders band propagates faster in the tensile direction with increasing thickness.
- The top band propagates downwards faster that the bottom band propagates upwards
- The angle the Lüders band forms with respect to the vertical loading axis increases with increasing thickness.
- All samples regardless of thickness exhibited the formation of two simultaneous bands at the two shoulders of the specimen
- The Lüders top band nucleated and formed prior to the bottom band. This is associated here with the samples being pulled in tension from the top grip (crosshead) while being held stationary from the bottom grip.
- The top band was more pronounced and had a higher strain magnitude compared to the bottom band

Worth noting that the preliminary results and findings of the experimental work were presented at the Society of Experimental Mechanics' 2022 annual conference [31]. A paper on this work has been submitted to Experimental Mechanics for publication and is currently under review as of October 31, 2022. The work here can be extended in the future by investigating:

- Using hydraulic grips as opposed to manual wedge grips to eliminate the introduction of any stress concentration from twisting the samples. This would certainly help get clarity on the locations of the nucleation.

- Performing the same test but with two DIC systems recording data simultaneously. One DIC camera facing the front of the specimen and the other camera facing the edge of the sample. This would help get a better idea on the propagation of the Lüders band from the core of the sample outwards towards the surface prior its motion in the vertical loading direction.

- While the sample thickness was investigated here, equally important is the sample geometry. A similar type of investigation can be carried out with respect to various geometries (namely rectangular and circular). This would further provide insights on the nature of the Lüders formation phase.

# References


[1] V. Ananthan and E. Hall, "Macroscopic aspects of Lüders band deformation in mild steel," *Acta Metallurgica et Materialia,* vol. 39, no. 12, pp. 3153-3160, 1991.

[2] S. Kyriakides and J. E. Miller, "On the Propagation of Luders Bands in Steel Strips," *Journal of Applied Mechanics,* vol. 67, no. 4, pp. 645-654, 2000.

[3] R. Onodera, M. Nonomura and M. Aramak, "Stress Drop, Luders Strain and Strain Rate during Serrated Flow," *Journal of the Japan Institute of Metals and Materials,* vol. 64, no. 12, pp. 1162-1171, 200.

[4] S. Nagarajan, R. Narayanaswamy and V. Balasubramaniam , "An Insight into Lüders Deformation Using Advanced Imaging Techniques," *Journal of Materials Engineering and Performance,* vol. 22, pp. 3085-3092, 2013.

[5] A. Cottrell and B. Bilby, "Dislocation Theory of Yielding and Strain Ageing of Iron," in *Proceedings of the Physical Society, Section A, Volume 62, Number 1*, 1949.

[6] S. Rešković, I. Jandrlić and F. Vodopivec, "Influence of Testing Rate on Lüders Band Propagation in Niobium Microalloyed Steel," *Metalurgija,* vol. 55, no. 2, pp. 157-160, 2016.

[7] Y.-L. Cai, S.-L. Yang, S.-H. Fu and Q.-C. Zhang, "The Influence of Specimen Thickness on the Lüders Effect of a 5456 Al-Based Alloy: Experimental Observations," *Metals*, vol. 6, no. 5, p. 120, 2016.

[8] H. B. Sun, F. Yoshida, M. Ohmori and X. Ma, "Effect of strain rate on Lüders band propagating velocity and Lüders strain for annealed mild steel under uniaxial tension," *Materials Letters,* vol. 57, pp. 4535-4539, 2003.

[9] W. Sylwestrowicz and E. Hall, "The deformation and ageing of Mild steel," *Proceedings of the Physical Society. Section B,* vol. 64, no. 6, pp. 495-502, 1951.

[10] J. Zhang and Y. Jiang, "Luders bands propagation of 1045 steel under multiaxial stress state," *Materials Letters,* vol. 21, pp. 651-670, 2005.

[11] T. Brlić, S. Rešković, F. Vodopivec and I. Jandrlić, "Lüders Bands at the Beginning of the Plastic Flow of Materials," *Metalurgija,* vol. 47, no. 10, pp. 357-359, 2018.

[12] S. C. Ren, T. F. Morgeneyer, M. Mazière and S. Forest, "Effect of Lüders and Portevin–Le Chatelier localization bands on plasticity and fracture of notched steel specimens studied by DIC and FE simulations," *International Journal of Plasticity,* vol. 136, p. 102880, 2021.

[13] P. M. N. M. B. Reyne, "Macroscopic consequences of Piobert–Lüders and Portevin–Le Chatelier bands during tensile deformation in Al-Mg alloys," *Materials Science & Engineering A,* vol. 746, pp. 187-196, 2019.

[14] P. M. H. L. M. O. L. M. J. Coër, "Piobert–Lüders plateau and Portevin–Le Chatelier effect in an Al–Mg alloy in simple shear," *Mechanics Research Communications,* vol. 48, pp. 1-7, 2013.

[15] M. Mazière, C. Luis, A. Marais, S. Forest and M. Gaspérini, "Experimental and numerical analysis of the Lüders phenomenon in simple shear," *International Journal of Solids and Structures*, vol. 106, pp. 305-314, 2017.

[16] S. Avril, F. Pierron, M. Sutton and J. Yan, "Identification of elasto-visco-plastic parameters and characterization of Lüders behavior using digital image correlation and the virtual fields method," *Mechanics of Materials*, vol. 40, pp. 729-742, 2008.

[17] F. Yoshida, "A constitutive model of cyclic plasticity," *International Journal of Plasticity*, vol. 16, pp. 359-380, 2000.

[18] D. H. Johnson, "Lüders Bands in RPV Steel," in *Ph.D Dissertation, Department of Eng. and Appl. Sc., Cranfield University*, Cranfield, 2012.

[19] ASTM, "ASTM E415-21: Standard Test Method for Analysis of Carbon and Low-Alloy Steel by Spark Atomic Emission Spectrometry," ASTM International, 2021.

[20] ASTM, "Standard Test Methods for Determining Average Grain Size," ASTM International, 2021.

[21] N. Tsuchidaa, H. Masuda, Y. Harada, K. Fukaura, Y. Tomato and K. Nagai, "Effect of ferrite grain size on tensile deformation behavior of a ferrite-cementite low carbon steel," *Materials Science and Engineering: A*, vol. 488, no. 1-2, pp. 446-452, 2008.

[22] ASTM, "ASTM E8/E8M-22: Standard Test Methods for Tension Testing of Metallic Materials," ASTM International, 2022.

[23] Correlated Solutions, Inc., *Vic-3D 9.2 Manual.*

[24] Correlated Solutions, Inc., *Vic-3D 9 Testing Guide.*

[25] Correlated Solutions, Inc., *CSI Application Note AN-525.*

[26] N. Tsuchida, Y. Tomato, K. Nagai and K. Fukaura, "A simple relationship between Lüders elongation and work-hardening rate at lower yield stress," *Scripta Materialia,* vol. 54, no. 1, pp. 57-60, 2006.

[27] H. Qiu, T. Inoue and R. Ueji, "Experimental measurement of the variables of Lüders deformation in hot-rolled steel via digital image correlation," *Materials Science & Engineering a,* vol. 790, p. 139756, 2020.

[28] H. Qiu, T. Inoue and R. Ueji, "In-Situ Observation of Lüders Band Formation in Hot-Rolled Steel via Digital Image Correlation," *Metals,* vol. 10, no. 4, p. 530, 2020.

[29] B. S. Shariat, Y. Li, H. Yang, Y. Wang and Y. Liu, "On the Lüders band formation and propagation in NiTi shape memory alloys," *Journal of Materials Science & Technology*, vol. 116, pp. 22-29, 2022.

[30] D. Johnson, M. Edwards and P. Chard-Tuckey, "Microstructural effects on the magnitude of Lüders strains in a low alloy steel," *Materials Science and Engineering: A*, vol. 625, pp. 36-45, 2015.

[31] J. H. van der Heijde and W. A. Samad, "The Influence of Specimen Thickness on the Lüders Effect in Mild Steel: Experimental Observations using DIC," in *SEM Annual Conference & Exposition on Experimental & Applied Mechanics*, Pittsburgh, PA, 2022.